BINDURA UNIVERSITY OF SCIENCE EDUCATION FACULTY OF SCIENCE AND ENGINEERING CHEMISTRY DEPARTMENT



USE OF CASSAVA WASTE NANOFIBRILS FOR ADSORPTION OF SELECTED SECOND-LINE ART DRUGS: ATAZANAVIR AND TENOFOVIR

LOVEMORE CHIWUNDURA MAKAZA (B211016B)

Supervisor: Dr N. MUCHANYEREYI

A DISSERTATION SUBMITTED IN PARTIAL FULFILMENT OF THE REQUIREMENTS OF THE BACHELOR OF SCIENCE HONOURS DEGREE IN CHEMICAL TECHNOLOGY (HBScCHT)

JUNE 2025

APPROVAL FORM

The undersigned parties confirm they supervised, read and endorse to the Bindura University of Science Education for the acceptance of a research dissertation entitled:

USE OF CASSAVA WASTE NANOFIBRILS FOR ADSORPTION OF SELECTED SECOND-LINE ART DRUGS: ATAZANAVIR AND TENOFOVIR

Submitted by Lovemore Chiwundura Makaza

In partial fulfilment of the requirements for the Bachelor of Science Honors Degree in Chemical Technology.

62	30/06/25
(Student)	(Date)
@M	30/06/25
(Supervisor)	(Date)
(Chairperson)	(Date

DECLARATION FORM

I the undersigned, Lovemore Chiwundura Makaza, assert to the Bindura University of Science Education that this dissertation is my original work and all academic sources incorporated to my own has been recognized and cited. I also declare the current work has not been presented to any educational institution for any educational merit purposes.

	(a)
Signature .	0 00

30/06/25 Date.....

DEDICATIONS

This masterpiece is dedicated to my father, friends and siblings, their invaluable financial support has been fundamental to my pursuit of becoming a chemical technologist and chemical engineer. Your belief in my aspirations and your generous contributions have paved the way for this achievement, and for that, I am eternally grateful.

ACKNOWLEDGEMENTS

Firstly, I thank the Lord for giving me vision and strength to overcome this battle. Would also like to take this opportunity to appreciate all my friends and loved ones that assisted in different ways. I also wish to express my sincere gratitude to several individuals whose contributions were essential to the completion of this project. My thanks go to Vincent at the University of Johannesburg, South Africa, for generously granting access to their instruments, which was vital for the characterization of my synthesized samples. I am also deeply thankful to Mam R. Zhou, Lab Technician at Bindura University, for her invaluable expert assistance, guidance, and opinions. Also, the laboratory personnel, for allowing the initial research exercises and experiments detailed in this text to be carried out in the university laboratory. Furthermore, I extend my profound appreciation to my academic mentor and supervisor, Dr. N. Muchanyereyi, for her crucial assistance, insightful opinions, and dedicated supervision, which were instrumental in bringing this academic context to its best possible form.

ABSTRACT

Utilizing agricultural waste into low cost-effective adsorbents presents a sustainable solution to the growing challenge of pharmaceutical water contamination. In this current study, nanocellulose and lignin-containing cellulose nanofibrils were synthesized from cassava waste using alkali treatment followed by partial bleaching process and mechanical homogenization. Lignin containing cellulose nanofibrils were used as the adsorbent after characterized using Fourier-Transform Infrared spectroscopy, X-ray Diffraction, Thermogravimetric Analysis, and Scanning Electron Microscopy with Energy-Dispersive Xray Spectroscopy followed by the evaluation for the effective adsorption of the selected second-line antiretroviral drugs, Atazanavir and Tenofovir. Fourier-Transform Infrared analysis confirmed the successful biosorption of Atazanavir and Tenofovir, revealing prominent shifts in the amide and aromatic regions (1650-1500 cm⁻¹) on the drug-loaded adsorbent. X-ray diffraction analysis showed a stable pattern even after adsorption proving that the adsorbent is structurally robust, confirming that adsorption occurs on the surface without damaging the material's core, which is essential for its durability. Thermogravimetric analysis confirmed the thermal stability of the adsorbent, and significantly, the Lignin-containing cellulose nanofibrils demonstrated superior purity with a final ash content below 1%, compared to the raw peel. Scanning electron micrographs revealed a highly porous, layered microstructure that became visibly smoother after sorption, while Energy-Dispersive X-ray spectroscopy confirmed the adsorbent is primarily composed of carbon (54.5 Wt%) and oxygen (45.3 Wt%). The data modelling followed the pseudo-second-order kinetics, indicating chemisorption was the rate limiting step in the adsorption process. The adsorption process for both drugs fitted the Freundlich isotherm model suggesting adsorption on a heterogeneous surface. Thermodynamic analysis confirmed the process is endothermic, spontaneous, and entropy-driven. Future work should focus on competitive adsorption studies and put attention to regeneration studies.

TABLE OF CONTENTS

APPROVAL FORM	i
DECLARATION FORM	ii
DEDICATIONS	iii
ACKNOWLEDGEMENTS	iv
ABSTRACT	v
List of figures	X
List of Tables	xi
Key words	xii
Abbreviations	xii
CHAPTER 1: INTRODUCTION	1
1.1 Background	1
1.2 Problem Statement	2
1.3 Aim	3
1.4 Specific Objectives	3
1.5 Problem Justification	3
1.6 Significance of Research	4
1.7 Delimitation of the Research	5
CHAPTER 2 : LITERATURE REVIEW	6
2.1 Pharmaceutical contaminants and Advanced Adsorption	6
2.1.1 Efficiency of Different Adsorbents in synthetic waters	6
2.1.2 Limitations of Conventional Treatment Methods	6
2.2 Methods for lignin containing cellulose nanofibrils synthesis	7
2.2.1 Top-Down Method	8
2.2.1.1 Mechanical Treatments	8
2.2.1.2 Chemical Pretreatments	8

2.2.2 Bottom-Up Method	8
2.2.2.1 Bacterial Nanocellulose (BNC)	8
2.2.2.2 Electrospinning	8
2.2.3 Hybrid Methods	9
2.3 Partially bleached, Lignin containing CNFs (As a Tailored Adsorbent)	9
2.4 Characterization Methods of LCNFs	10
2.5 Target Adsorbates: Atazanavir (ATV) & Tenofovir (TFV)	12
2.5.2 Thermodynamic Considerations of Atazanavir and Tenofovir	13
2.6 Adsorption Equilibrium (Isotherms)	13
2.6.1 Langmuir Isotherm	14
2.6.2 Freundlich Isotherm	14
2.7 Thermodynamics and Kinetic Analysis	14
CHAPTER 3: MATERIALS AND METHODS	15
3.1 Synthesis of LCNFs	15
3.2.0 Characterization	17
3.2.1 Fourier Transform Infrared Spectroscopy (FTIR)	17
3.2.2 X-ray diffraction (XRD)	18
3.2.3 Thermogravimetric Analysis (TGA)	18
3.2.4 Point of zero charge (pHpzc) determination	18
3.2.5 Scanning Electron Microscopy (SEM-EDS) analysis	19
3.2.6 Chemical composition	19
3.3 Preparation of stock solutions	20
3.5.0 Adsorption	21
3.5.1 Effect of adsorbent dosage	21
3.5.2 Effect of pH	21
3.5.3 Effect of temperature	22

3.5.4 Effect of contact time	22
3.6 Data treatment methods	22
3.6.1 Removal capacity and adsorption capacity	22
3.6.2 Adsorption Isotherms	23
3.6.3 Adsorption kinetics	24
3.6.4 Thermodynamics	24
CHAPTER 4: RESULTS AND DISCUSSION	25
4.1 Percentage yield and purity	25
4.2 Characteristics of raw Cassava Peel (CP), Nanocellulose (NC) and Synthesized	
	25
4.2.1 Physico-chemical characteristics of raw CP and synthesized adsorbent	25
4.2.2 Surface morphology and elemental composition	26
4.2.2.1 Cassava Peel (CP)	26
4.2.2.2 Nanocellulose (NC)	27
4.2.2.3 Lignin Cellulose Nanofibrils (LCNFs)	28
4.2.2.4 Before and After Adsorption Scanning Electron Microscopy (SEM) Co	omparison
	29
4.2.3 Thermogravimetric Analysis (TGA)	31
4.2.4 Fourier Transform Infrared Spectroscopy Analysis (FTIR)	32
4.2.5 X-ray diffraction Analysis (XRD)	33
4.3 Effects of Experimental Conditions	35
4.3.1 Adsorbent dosage	35
4.3.2 Temperature	35
4.3.3 pH	36
4.3.4 Contact Time	36
4.4 Isothermic modelling	37
4.5 Adsorption Kinetics	38

4.6 Adsorption thermodynamics	41
4.7 Mechanism of adsorption	43
CHAPTER 5: CONCLUSION AND RECOMMENDATIONS	45
5.1 Conclusion	45
5.2 Recommendations	46
References	47
Appendix	55

List of figures

Figure 2.1 :Chemical structure of ATA
Figure 2.2: Chemical structure of TFV
Figure 3.1 : Synthesis of LCNFs flow process
Figure 4.1 : SEM micrograph (left) and corresponding SEM-EDX
Figure 4.2 : SEM micrograph (left) and corresponding SEM-EDX
Figure 4.3: SEM micrograph (left) and corresponding SEM-EDX
Figure 4.4 : SEM micrographs at 20µm, Before(left) & After (right) adsorption30
Figure 4.5 : SEM micrographs at 50µm both after adsorption
Figure 4.6 : SEM micrographs at 100μm, Before(left) & After (right) Adsorption31
Figure 4.7: TGA thermograms for raw CP, NC & LCNFs
Figure 4.8 :FTIR Spectra of raw CP, NC and LCNFs (left) before sorption and (right) after sorption of ATA using LCNFs1 and TFV using LCNFs2
Figure 4.9: XRD diffractograms of raw CP, NC and LCNFs before (left) and after (right) adsorption of ATA using LCNFs1 and TFV using LCNFs2
Figure 4.10: Experimental conditions: effect of contact time (a), effect of pH (b), effect of dosage (c) and effect of temperature (d)
Figure 4.11: Langmuir model for the adsorption of ATA (a), Freundlich model for the adsorption of ATA (b), Langmuir model for the adsorption of TFV (c) and Freundlich model for the adsorption of TFV (d)
Figure 4.12 : pseudo-first-order (a, c) and pseudo-second-order (b, d) for the adsorption of TFV and ATA
Figure 4.13: Van't Hoff plot for ATA (left) and TFV (right)
Figure 4.14 : Schematic diagram of the mechanisms involved in the sorption of TFV & ATA on LCNFs shown on an after-adsorption SEM micrograph

List of Tables

Table 2.1 : Comparison of Advanced Treatment Technologies for Micropollutant Removal .	7
Table 2.2: Adsorption Mechanisms.	10
Table 2.3 : Comparison of Adsorption Capacities	10
Table 2.4 : Comparison of ATA and TFV	13
Table 4.1 : Comparison of raw CP , anocellulose and LCNFs	26
Table 4.2 : Adsorption Isotherm and Reaction Kinetics Parameters	40
Table 4.3 :Thermodynamic parameters of the adsorption of ATA and TFV on LCNFs	42
Table 4.4: Comparison of the adsorbent under study with those from literature	44

Key words

- 1. Antiretroviral
- 2. Adsorbent
- 3. Atazanavir
- 4. Tenofovir
- 5. Nanocellulose
- 6. Isotherm
- 7. Cassava
- 8. Kinetics

Abbreviations

- 1. ECs Emerging Contaminants
- 2. CNFs Cellulose Nanofibrils
- 3. ATA Atazanavir
- 4. TFV Tenofovir
- 5. ARVDs Antiretroviral drugs
- 6. SEM-EDS Scanning Electron Microscopy Energy Dispersive Spectroscopy
- 7. CP Cassava Peel
- 8. WWTPs Wastewater Treatment Plants
- 9. Rpm Revolutions per minute
- 10. LCNFs Lignin Cellulose Nanofibrils
- 11. API Active Pharmaceutical Ingredients
- 12. AOPs Advanced Oxidation Processes
- 13. RQs Risk Quotients

CHAPTER 1: INTRODUCTION

This chapter gives a background overview of the problem at hand and the proposed solution to the research.

1.1 Background

Many emerging contaminants (ECs) pollute worldwide water supplies, posing an increasing environmental threat (Sharma et al., 2024). Due to their natural biological effectiveness, active pharmaceutical ingredients (APIs), also known as pharmaceuticals and personal care products (PPCPs), are particularly concerning (Sharma et al., 2024). Municipalities and hospitals are the main sources of pharmaceutical pollution.

These chemicals persist and are biologically active, therefore conventional treatment methods generally fail (Baaloudj et al., 2024; Khan & Barros, 2023). Pharmaceutical contamination occurs when unwanted or expired drugs are dumped in sewers or landfills. The chemicals can seep into groundwater and surface water (Baaloudj et al., 2024). APIs and other byproducts from pharmaceutical factories often go untreated (Nassri et al., 2023). Pharmaceuticals can also enter aquatic systems through natural pathways, such as excretion by humans and animals, with some compounds persisting in the environment due to their resistance to biodegradation (Baaloudj et al., 2024; O'Flynn et al., 2021). Due to their biological strength and often lengthy breakdown periods lead to possible ecological effects even at very low levels (typically in the ng/L to µg/L range(Wilkinson et al., 2022).

Traditional WWTPs lack the advanced monitoring tools necessary to detect and quantify micropollutants at trace levels. Without effective monitoring, it becomes challenging to implement targeted treatment strategies, further complicating the removal of these contaminants (Bracamontes-Ruelas et al., 2025; Jaria et al., 2023). Biological treatment techniques, such as activated sludge systems, often achieve only a partial reduction of these pesky contaminants, as many medicines show low biodegradability or may even be harmful to the tiny organisms that are essential to the treatment processes (Ndlangamandla et al., 2018).

Considering the inherent constraints associated with conventional approaches, a multitude of novel technologies has been examined, encompassing sophisticated oxidation procedures (SOPs), ozonation, and membrane separation techniques (such as nanofiltration and reverse osmosis) (Bilal et al., 2021). While these advanced methods can help improve removal

efficiencies for pharmaceuticals, they are often weighed down by some notable downsides, such as high operational costs, considerable energy demands, technical complexities, membrane fouling challenges, and the possibility of creating harmful by-products or transformation products, which may, in some cases, be more toxic than the original compounds (Karak et al., 2024).

Adsorption has come forward as a well-studied and very promising alternative or complementary technology for treatment of a wide range of pollutants, including pharmaceuticals, from water sources (Bilal et al., 2021). The advantages of this approach include operational simplicity, high efficiency even at low contaminant levels, cost-effectiveness compared to many advanced methods, the potential for adsorbent regeneration and recycling, and the prevention of harmful by-product formation.

Nanocellulose, derived from agricultural waste like cassava peels, have gained significant attention as sustainable, budget-friendly, and incredibly effective adsorbents due to their large surface area, biodegradability, and functional groups that boost pollutant attraction (Phanthong et al., 2018). Using cassava waste for LCNFs production aligns well with economy principles by transforming agro-industrial by-products into valuable materials.

1.2 Problem Statement

Commonly prescribed second line ARVDs, atazanavir (ATA) an HIV protease inhibitor and tenofovir (TFV) a nucleotide reverse transcriptase inhibitor, both of which have been found in environmental water samples (Nannou et al., 2020). As both are second-line ART medications, their presence in water samples can be linked to their current higher use following non-adherence to first-line treatment guidelines. The presence of ARV drugs in surface waters poses potential risks to aquatic ecosystems and human health, for instance TFV, has shown to exhibit genotoxic effects on aquatic organisms, with risk quotients (RQs) exceeding the threshold of 1, indicating significant environmental concern (Ngwenya & Musee, 2023). ATA accumulates in contaminated soil crops, raising food chain exposure issues (Dube & Nindi, 2020). ARV medications increase antimicrobial resistance by selectively pressuring microbial communities in wastewater treatment plants and surface waterways. ARVDs are environmentally persistent pollutants. In aquatic biodegradation, several ARVDs, including TFV, survive (Nannou et al., 2020). Activated carbon filtration and advanced oxidation are costly or pollute (Dolar et al., 2016). A cost-effective, eco-friendly, and scalable adsorbent is

needed to remove pharmaceutical pollutants. Cassava waste-derived Lignin containing CNFs offer a promising yet underutilized solution for this issue.

1.3 Aim

To investigate the feasibility and efficiency of using partially bleached CNFs retaining lignin, extracted from cassava waste, as a bio-adsorbent for the removal of ATA and TFV from synthetic polluted water samples under controlled laboratory conditions.

1.4 Specific Objectives

To achieve the overall aim, the following have been defined:

- To extract lignin containing CNFs from cassava waste using Top-Down Method.
- To characterize the synthesized LCNFs using fourier transform infrared spectroscopy (FTIR), x-ray diffraction (XRD), scanning electron microscopy (SEM-EDS), point of zero charge (pHpzc) determination, and thermogravimetric (TGA) analysis to determine key physicochemical properties relevant to adsorption, such as surface functional groups, crystallinity, morphology, elementary composition of the LCNFs and fibril dimensions.
- To determine the equilibrium adsorption capacity (qe) of the LCNFs for ATA and TFV individually in aqueous solutions under controlled laboratory conditions.
- To investigate the influence of key operational parameters, specifically initial solution pH, contact time, temperature and initial drug concentration on the adsorption efficiency of ATA and TFV onto the synthesized LCNFs.
- To evaluate the kinetics of the adsorption process by fitting experimental data to pseudo-first-order and pseudo-second-order kinetic models, determining relevant rate constants.
- To analyze the equilibrium adsorption data using Langmuir and Freundlich isotherm models to determine maximum adsorption capacities (q_{max}) and gain insights into the adsorption mechanism.

1.5 Problem Justification

Africa, a continent heavily impacted by the HIV epidemic and high ARV usage, produces millions of tonnes of cassava processing waste annually, so using it to make LCNFs aligns with

economy goals and turns a low-value byproduct into an environmentally friendly material (Widiarto et al., 2019).

The existence of antiretroviral medications in aquatic systems endangers aquatic life and lead to the emergence of drug-resistant HIV variants (Singer et al., 2016). In Zimbabwe no studies have been conducted in relation to these ARVDs, yet it's one of the countries with high usage of these drugs in Southern Africa. When these drugs reach the water sources creates the perfect breeding ground for drug-resistant strains to evolve. The viruses that happen to have random mutations allowing them to survive these low doses will multiply, passing on their resistance. Natural polymer cellulose is renewable, abundant, and biodegradable. Using this long chain polymer and its elementary fibrils with dimensions from 10 to 350 nm can create a new adsorbent for this problem. Nanocellulose from plants and its modified forms have been studied for adsorbing heavy metals and pharmaceuticals (Liu et al., 2022).

The novelty of this study lies specifically in investigating the adsorption performance of partially bleached CNFs retaining lignin derived specifically from CP. Retaining lignin reduces excessive chemical exposure to reserve the fibrils structure, also balances H – bonding (TFV) and π – π stacking (ATA) for efficient adsorption . Most studies have synthesized CNFs using acid hydrolysis in the range concentration of 36–64 wt.% (S Widiarto, 2017) , in this research lignin containing CNFs were synthesized from CPs by eluding the acid hydrolysis step therefore minimizing the use of harsh chemical concentrations and reduce the cost production of CNF. This synergistic approach, where a solution to pollution is derived from managing waste and reduction of excessive chemicals usage, provides a powerful justification for the research.

1.6 Significance of Research

- Environmental protection by investigating a potential method for removing persistent ARVDs from water.
- Sustainable water treatment by utilizing agro-waste for nanomaterial synthesis.
- Development of sustainable adsorbents which are bio-based and renewable.
- Providing insights into the adsorption mechanisms of ARVs on LCNFs.
- Foundation for further research testing in real wastewater matrices and potential scaleup for practical application.

1.7 Delimitation of the Research

All experiments will be conducted under controlled laboratory conditions, pilot or industrial scale are not considered. Adsorption experiments will utilize synthetic aqueous solutions prepared by dissolving ATA and TFV standards in deionized water. The study focuses solely on ATA and TFV. Only LCNFs derived from cassava waste will be investigated.

CHAPTER 2: LITERATURE REVIEW

This chapter reviews literature to contextualize the investigation into using cassava wastederived nanofibrils containing lignin as effective adsorbents for the adsorption of selected ARVDs (ATA and TFV). The review will focus on these core areas, the problem of the ARVDs drugs in aqueous environments, similar adsorption studies that have been done, synthesis, properties, characterization of nanofibrils, the existing knowledge on nanocellulose materials applied to pollutant adsorption, including kinetic and equilibrium studies.

2.1 Pharmaceutical contaminants and Advanced Adsorption

The prevalence of ARVDs, particularly ATA and TFV in wastewater in Africa has been a growing concern due to their emergence as contaminants. Their increasing use in Africa has led to concerns about their presence in wastewater and surface waters. These drugs, ATA and TFV can enter the environment through incomplete metabolism in the human body, improper disposal of unused or expired medications, and insufficient wastewater treatment (Kudu et al., 2022; Adeola & Forbes, 2021). Advanced bio-sorbents, particularly those based on nanotechnology, offer promising solutions due to their high efficiency, low cost, and ease of application.

2.1.1 Efficiency of Different Adsorbents in synthetic waters

Since pharmaceuticals are becoming more detected in water and traditional wastewater treatment methods are limited, recent research has focused on using lignin-based bio-based adsorbents to remove them from synthetic polluted water samples. Hyperbranched Kraft lignin containing nitrogen atoms was used to increase active sites for adsorbing antibiotics and anti-inflammatory drugs at concentrations ranging from 5 to 150 μg/l. Drugs without chlorine or fluorine adsorb better by endothermic, spontaneous adsorption (Gomez-Ceballos et al., 2021). Electrically spun lignin nanofibers absorb fluoxetine from water. These 156-nm nanofibers removed 32 ppm of contaminants 70% effectively. Heavy metal ions and antibiotics are well-absorbed by PAL microparticles. Levofloxacin hydrochloride at 80 mg/l was removed 99.91% by PAL. During sorption, π-π stacking, hydrogen bonding, and electrostatic interactions occurred (Gong et al., 2021).

2.1.2 Limitations of Conventional Treatment Methods

Activated sludge processes often fail to remove pharmaceutical contaminants like ARVDs. These pollutants are released into the environment due to this inadequacy (Eryildiz et al., 2022). ARVD transformation products can be more persistent and toxic than the parent compounds,

making removal more difficult (Eryildiz et al., 2022). ARV drugs like Nevirapine and Efavirenz are pharmacologically active at low concentrations, making them problematic in wastewater. These drugs persist in wastewater because they are excreted in their active form (Le et al., 2020). Due to their hydrolysis resistance and poor biodegradability, conventional biological treatments fail (Gupta et al., 2024). Lack of standardised treatment protocols hinders ARV drug removal from wastewater, especially in Zimbabwe. Promising advanced oxidation processes (AOPs) and other tertiary treatments face integration challenges due to high costs and operational complexity in existing WWTPs (Pratiwi et al., 2025; Kulišťáková, 2023).

Table 2.1: Comparison of Advanced Treatment Technologies for Micropollutant Removal

Technology	Key Advantages	Limitations	Reference
Advanced Oxidation Processes (AOPs)	High oxidation efficiency, mineralization of pollutants	High energy consumption, formation of byproducts	(Pratiwi et al., 2025; Bisognin et al., 2023; Oturan & Oturan, 2024)
Membrane Filtration	High removal efficiency, size exclusion	High capital and maintenance costs	(Meghea et al., 2024; Thakre et al., 2024)
Activated Carbon Adsorption	Effective for a wide range of micropollutants	Requires frequent regeneration, high cost	(Meghea et al., 2024; Thakre et al., 2024; Ratchnashree et al., 2023)
Integrated Treatment Systems	Synergistic effects, reduced by-product formation	Complex operation, high initial investment	(Pratiwi et al., 2025; Bracamontes-Ruelas et al., 2025; Kulišťáková, 2023)

2.2 Methods for lignin containing cellulose nanofibrils synthesis

The synthesis of nanofibrils can be broadly categorized into two main approaches: top-down and bottom-up methods.

2.2.1 Top-Down Method

The top-down approach involves the mechanical or chemical disintegration of natural cellulose fibers into nanofibrils. This method typically starts with raw cellulose sources, such as wood, bamboo, or agricultural residues, and uses various mechanical and chemical treatments to break down the fibers into nano-scale fibrils.

2.2.1.1 Mechanical Treatments

Mechanical treatments are the most common top-down methods for nanofibrils production. These include grinding, ultrasonication, high-pressure homogenization, and microfluidization. Nanofibrils form when intense mechanical forces disrupt cellulose fibre hydrogen bonds. In grinding treatment, cellulose fibres are reduced to nanofibrils with a mean width that is thicker than that of untreated pulp (Hwang et al., 2023).

2.2.1.2 Chemical Pretreatments

Chemical pretreatments and mechanical methods improve fibrillation efficiency. NaOH pretreatment solubilises hemicellulose and reduces hydrogen bonding between cellulose fibres, facilitating nanofibril disintegration. Also, TEMPO-mediated oxidation has been used to introduce carboxyl groups on cellulose fibres, improving dispersibility and CNF production (Miao et al., 2024; Khadraoui, 2022).

2.2.2 Bottom-Up Method

Bottom-up cellulose nanofibril synthesis from glucose or other cellulose precursors uses biological or chemical assembly. Although rarer than top-down, this method controls fibril structure better.

2.2.2.1 Bacterial Nanocellulose (BNC)

BNC is one of the most used bottom-up methods for CNFs production. BNC is synthesized by bacteria, such as *Gluconacetobacter xylinus*, through fermentation. The bacteria secrete cellulose nanofibrils forming a hydrogel. It is known for high purity, crystallinity, and mechanical strength, making it suitable for biomedical and electronic applications (Rostamabadi et al., 2024; Hsieh, 2018).

2.2.2.2 Electrospinning

Bottom-up electrospinning creates cellulose nanofibrils using electric fields. When cellulose is exposed to an electric field, a jet forms that solidifies into nanofibers. Electrospinning produces functional nanofibers with precise diameter and structure control (Kramar & González-Benito, 2022; Hsieh, 2018).

2.2.3 Hybrid Methods

Mixing top-down and bottom-up methods overcomes their drawbacks. Combine mechanical and enzymatic treatments to boost CNF yield and properties. Pretreatment with deep eutectic solvents (DESs) increases CNF production efficiency (Baraka et al., 2024; Peng et al., 2023). Recent hybrid and bottom-up methods provide high fibril structure control but are expensive, especially for large-scale synthesis. Top-down methods are cheaper bulk manufacturing because they are scalable, output high, and adaptable for industrial-scale adsorption production. This study uses top-down method

2.3 Partially bleached, Lignin containing CNFs (As a Tailored Adsorbent)

The presence of lignin in CNFs introduces a broader range of functional groups, including phenolic hydroxyl (which are generally more acidic and reactive than alcoholic), as well as its abundant aromatic structures, carboxylic, and aliphatic hydroxyl groups, which play a critical role in adsorption. These groups can facilitate electrostatic interactions, hydrogen bonding, and π - π interactions with pollutants (Tkachenko et al., 2025; Chen et al., 2018). Aromatic rings in lignin can engage in π - π interactions with aromatic pollutants, the targeted ATA and TFV further enhancing adsorption capacities. This mechanism is particularly relevant for the removal of organic dyes and pharmaceuticals (Tkachenko et al., 2025; Agustin et al., 2024).

Fully bleached CNFs rely on cellulose hydroxyl groups, which interact less diversely. Because lignin is retained, nanofibrils with lignin have multi porosity and surface area, creating void spaces and active adsorption sites. For instance, lignin-based porous super particles with 1152 m²/g surface area are effective for CO₂ capture and other adsorption applications (Zhao et al., 2021). As a natural binder, lignin boosts CNF-based materials' mechanical strength. Dynamic systems require mechanical stability for adsorbents (Morcillo-Martín et al., 2022; Chen et al., 2018).

High specific surface area is key to LCNF drug adsorption. Increased CNF surface area may improve drug loading (Garrido-Miranda et al., 2024; Lombardo, 2018). Controlled drug release from LCNF pores (Huo et al., 2022; Lunardi, 2021).

Neutral and cationic drugs adsorb better in laccase-crosslinked lignin containing nanocellulose cryogels. Crosslinking stabilised adsorbent by reducing lignin nanoparticle leaching (Agustin et al., 2024). Cassava waste-derived lignin-containing nanofibrils have not been utilized for adsorption despite their cost-effective and sustainability.

Table 2.2: Adsorption Mechanisms

Mechanism	Pure CNFs	Partially Bleached (contains lignin CNFs)
Hydrogen bonding	✓	✓
Electrostatic interactions	Limited	Enhanced
Hydrophobic effects	Minimal	Significant
π-π stacking	None	Present (lignin aromatic rings)
Pore filling	✓	✓

Table 2.3: Comparison of Adsorption Capacities

Pollutant Type	Lignin- Nanocellulose	Bleached Nanocellulose	Reference
Cationic Dyes	79-102µmol/g	50-70μmol/g	(Tkachenko et al., 2025)
Heavy Metals (Cd2+)	129.87mg/g	50-70mg/g	(Elsayed et al., 2023)
Pharmaceuticals	400% increase	_	(Agustin et al., 2024)

2.4 Characterization Methods of LCNFs

In order to optimise LCNF adsorption, it is necessary to understand their chemical, mechanical, thermal, and structural characteristics. Various properties of the particles are described, including their size, shape, crystallinity, and surface chemistry.

2.4.1 Microscopy Techniques

The use of microscopy is crucial for the structural and morphological examination of LCNF. The size, shape, and surface topography of nanofibrils can be determined using these techniques.

2.4.1.1 Scanning Electron Microscopy with Energy Dispersive Spectroscopy (SEM-EDS)

The morphology and elemental composition of LCNFs are characterized using SEM-EDS. Using SEM, researchers can examine LCNF surface morphology in great detail, allowing them to analyse structural features such as surface texture, length, and diameter. This is essential for comprehending the physical characteristics and applications of LCNFs (Yue et al., 2021). Elements of LCNF can be more readily detected and quantified using SEM-EDS.

2.4.2 Spectroscopy Methods

These techniques give critical insights into the functional groups, crystallinity, and molecular interactions within the nanofibrils, they provide valuable information about the functional groups, crystallinity, and molecular interactions in the nanofibrils.

2.4.2.1 Fourier-Transform Infrared Spectroscopy (FTIR)

FTIR is a method for examining the chemical composition of LCNFs. It shows the functional groups present in the fibrils, including hydroxyl (-OH), carbonyl (C=O), and methoxy (-OCH3) groups. FTIR has been used to analyze the chemical composition of CNFs derived from diverse sources, including Stipa obtuse fibers, indicating the presence of cellulose and the elimination of lignin and hemicellulose (Chavez et al., 2023). FTIR has been utilized to examine the impact of various treatments, including acid hydrolysis and bleaching, on the chemical composition of CNFs (Radakisnin et al., 2020).

2.4.2.2 X-Ray Diffraction (XRD)

Gives information on crystalline structure, crystallinity index, and the impact of different treatments on these characteristics. The crystallinity index, crystalline structure, and treatment effects can be shown using X-Ray Diffraction (XRD). By revealing the effects of processing procedures on crystallinity and shape, XRD sheds light on the structural integrity and possible applications of LCNFs. The crystallinity of LCNF can be enhanced by mechanical and chemical treatments. The crystallinity index of nanocrystalline cellulose produced from water hyacinth fibres was found to be 73% after undergoing chemical and ultrasonic treatments (Asrofi et al., 2017).

2.5 Target Adsorbates: Atazanavir (ATV) & Tenofovir (TFV)

For adsorption studies to be conducted, it is crucial to conduct research on drug- adsorbent interaction prediction. This includes materials such as partially bleached CNFs.

2.5.1 Structural Analysis of Atazanavir and Tenofovir

2.5.1.1 Atazanavir (ATA)

Figure 2.1 : Chemical structure of ATA

Molecular weight of ATA is 704.85 g/mol. It has a central aromatic ring system and hydrophobic side chains, these hydrophobic groups make ATA undergo hydrophobic adsorption. This allows it to interact with LCNF hydrophobic regions.

2.6.1.2 Tenofovir (TFV)

Figure 2.2: Chemical structure of TFV

The molecular weight of TFV is 287.21 g/mol. Because of its phosphonate group, it is more hydrophilic than ATV and negatively charged at physiological pH. This charge enhances CNF adsorption by interacting with their functional groups (Hasan et al., 2020; Lombardo & Thielemans, 2018). The log(p) value of 0.64 indicates hydrophilia for TFV. Its negative charge at physiological pH allows electrostatic interactions with positively charged surfaces.

2.5.2 Thermodynamic Considerations of Atazanavir and Tenofovir

The adsorption process for ATV and TFV is expected to be endothermic, with the entropy increase and enthalpy increase. The spontaneity of the adsorption process is confirmed by a negative Gibbs free energy change (ΔG), a characteristic commonly observed in drug-CNF interactions (Lombardo & Thielemans, 2019). The thermodynamics of drug adsorption onto carbon nanofibers is generally defined by an increase in entropy, resulting from the liberation of surface-bound water molecules. This phenomenon has been documented in research concerning poorly soluble pharmaceuticals and CNFs (Lombardo and Thielemans, 2019; Lombardo et al., 2018).

Table 2.4: Comparison of ATA and TFV

Property	ATV	TFV	Reference
Molecular Weight	704.85 g/mol	287.21 g/mol	(Varghese et al., 2023; Hasan et al., 2020)
LogP Value	5.67 (Hydrophobic)	0.64 (Hydrophilic)	(Varghese et al., 2023; Hasan et al., 2020)
Dominant Interaction	Hydrophobic interactions	Electrostatic interactions	(Lombardo et al., 2018)
Thermodynamic Driving Force	Entropy-driven adsorption	Entropy-driven adsorption	(Lombardo & Thielemans, 2019)

2.6 Adsorption Equilibrium (Isotherms)

This study investigates surface adsorption using Langmuir and Freundlich isotherms. Adsorption isotherms show LCNF-ARVD interactions. Although ARV drug adsorption by LCNFs from any biomass is not specifically studied, antibiotic and other pharmaceutical compound adsorption studies can provide insights. Langmuir and Freundlich isotherms accurately describe biomass-based CNF adsorption of pharmaceutical compounds. Langmuir

and Freundlich isotherms have been used to describe pharmaceutical compound adsorption onto CNFs from various biomasses.

2.6.1 Langmuir Isotherm

Langmuir isotherm assumes monolayer adsorption with evenly accessible sites. This model is used in adsorption of systems dominated by physorption (Lombardo & Thielemans, 2019).

2.6.2 Freundlich Isotherm

On heterogeneous surfaces and multilayer, Freundlich isotherm describes adsorption. This model works well for adsorption on surfaces with different adsorbate affinities (Kumar et al., 2023). Ethylenediamine-modified CNFs adsorb amitriptyline (AMI) at 87.66 mg/g according to the Freundlich isotherm (Bezerra et al., 2017).

2.7 Thermodynamics and Kinetic Analysis

Thermodynamic and kinetic analysis determines ARV drug adsorption onto LCNFs. Typically, adsorption reaction feasibility is evaluated using thermodynamic parameters such as ΔG° , ΔH° , and ΔS° . These parameters show adsorption spontaneity and nature. Van't Hoff equations are used to calculate these parameters from adsorption isotherm data, thermodynamic parameters are related to the equation. A positive ΔG° indicates non-spontaneity, while a negative one indicates spontaneity (Lima et al., 2021). Similar systems show spontaneous, endothermic pharmaceutical compound adsorption onto CNFs, with positive entropy changes indicating disorder (Amen et al., 2024). Freundlich and Langmuir adsorption isotherm models calculate equilibrium constants. The right isotherm model is needed to calculate thermodynamic parameters accurately (Tran et al., 2021; Mabuza, 2022). Pharmaceutical compound adsorption onto CNFs is often described using pseudo-second-order kinetics. Our model assumes adsorption rate is proportional to sites. The model accurately described OTC, CAP, and CIP adsorption onto CNFs (Amen et al., 2024).

CHAPTER 3: MATERIALS AND METHODS

All chemicals used were analytical grades (AR), supplied by Blackpeck Scientific which is located at 1 Lawson Ave, Harare, Zimbabwe. The reagents and chemicals were used without further purification. Amber reagent bottles were used to store all prepared stock solutions and samples to avoid harmful ultraviolet (UV) radiation, which can degrade or decompose many substances, the amber color of the glass acts as a barrier. All preparations were done in a fume hood to minimize exposure and all water used was deionized.

3.1 Synthesis of LCNFs

3.1.1 Material

Cassava peels (CP) and bagasse were collected from a Mt Darwin farm dump which is located at the 180 km peg on the Harare - Mount Darwin Road (-16.56° S, 31.58° E).

The reagents and equipment used were:

NaOH; Autoclave; Homogenizer; Deionized water; pH meter; Magnetic stirrer; Hydrogen Peroxide; Centrifuge; Spatula; Vacuum Pump; Oven; Volumetric flasks; Büchner funnel; Filter Papers; Wash Bottles.

3.1.2 Isolation of cellulose

First, the cellulose from cassava peels was isolated. The peels were washed with deionized water to remove dirt and contaminants, separated from their outer skin, cut into smaller pieces, and milled into pulp after 4 days of air drying. The alkali treatment method was used (Widiarto et al., 2017) with modifications to improve yield and retention of lignin .100 g of dried pulp was heated at 70 °C for 1-2 hours on a magnetic stirrer with 2000 mL of 3% (w/v) sodium hydroxide (NaOH) solution prepared by dissolving the solid pellets (≥ 97% purity) in deionized water. The mixture was bleached for 1 hour with constant stirring at 80 °C with 1000 mL of 5% (w/v) hydrogen peroxide prepared by diluting a 30% (w/v) stock solution. The residue obtained was washed with distilled water until pH 7.

3.1.3 Determination of lignin content

To quantify the retained lignin in CNFs, the klason lignin method was used, following the general principles of the Klason method (TAPPI T 222 om-22, 2022). 3 g of dried LCNFs (W_1) were treated with 65% sulphuric acid(30 ml) at 30 $^{\circ}$ C for 1 hour in an auto clave. The insoluble

residue was vacuum filtered through a pre-weighed glass crucible (W_2) , washed with warm water at 40° C until acid-free, then dried at 100° C for 12 hours and reweighed the crucible (W_3) .

Triplicate samples of 3 g LCNFs were analyzed to obtain mean lignin retention using the equation 3.1:

lignin % =
$$\frac{W_3 - W_2}{W_1} \times 100$$
 (3.1)

3.1.4 Preparation of nanofibrils

LCNFs were prepared via mechanical disruption using the grinding process. This was started with a refined cellulose pulp dispersed in water to create a low-concentration slurry (Smith et al., 2021). This suspension was blended for an hour. The intense mechanical shear forces, compression, and friction caused the disintegration of the larger cellulose cell walls. The effect of multiple blending cycles successfully individualized the nanofibrils within the structure, ultimately yielding a stable aqueous suspension of LCNFs, with the degree of fibrillation often being controlled by adjusting the blending levels. The colloidal suspension of LCNFs prepared through blending was first centrifuged at 14,000 rpm at -4°C to form a gel. The LCNF gel was oven-dried at 40°C for 5 hours to remove moisture while preserving the fibrillar structure. The dried material was manually crushed using a mortar and pestle to obtain a fine, homogeneous powder (Kim et al., 2025).

3.1.5 Synthesis of Lignin containing Cellulose Nanofibrils



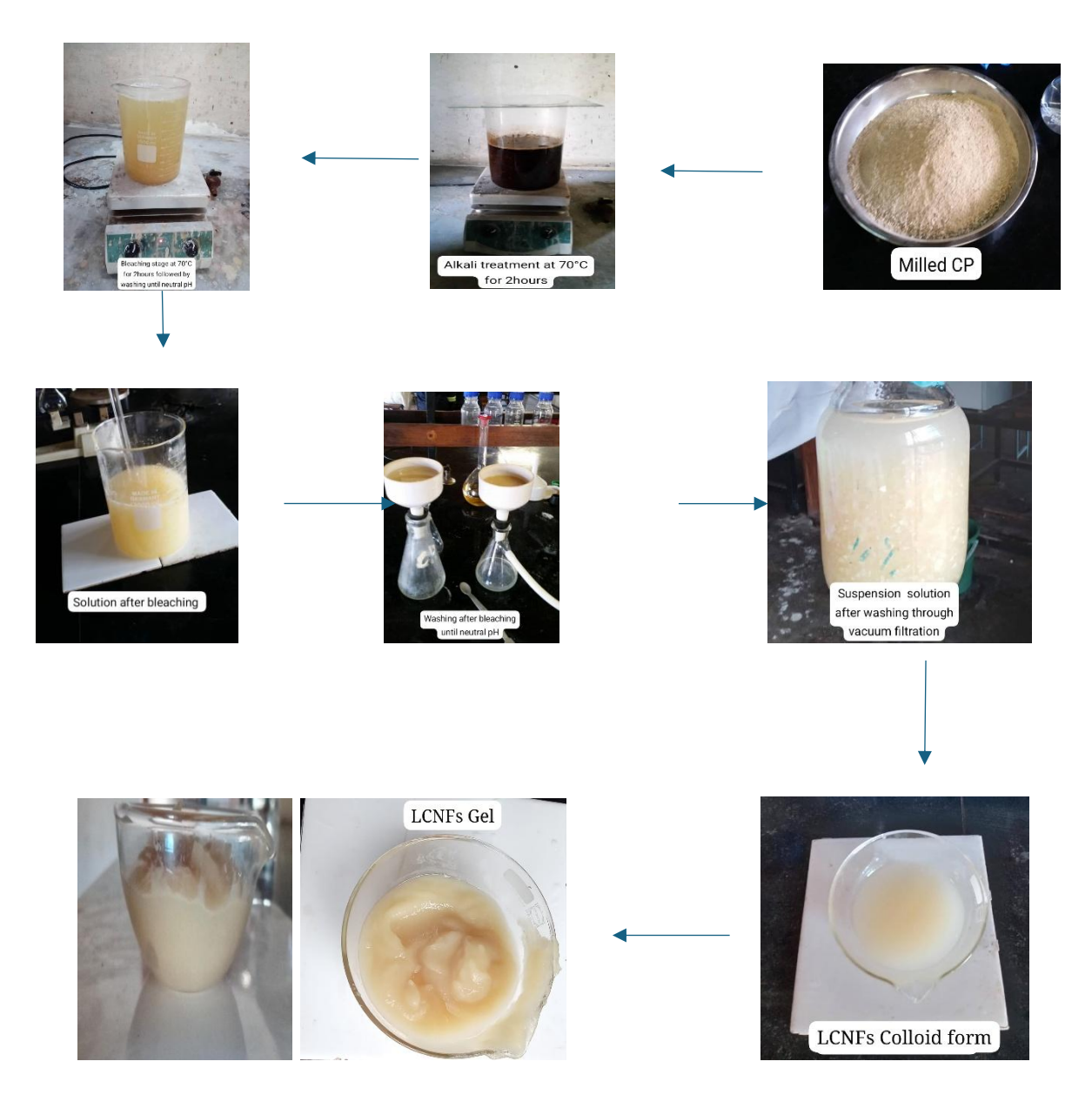


Figure 3.1: Synthesis of LCNFs flow process

3.2.0 Characterization

3.2.1 Fourier Transform Infrared Spectroscopy (FTIR)

Dried samples of CP, NC and LCNFs were analyzed, and functional groups involved on the physical surface were observed on an FTIR(Bruker Tensor 27, Shimadzu, Kyoto, Japan). A spatula was used to add samples of the CP, NC and LCNFs to the crystal on the FTIR, spectra were recorded for the adsorbent both before and after the adsorption process. This comparative analysis helps reveal the binding mechanisms between the adsorbent and the contaminant (Hlefane et al., 2021).

3.2.2 X-ray diffraction (XRD)

Freeze-dried raw CP, NC and LCNFs samples were put in suitable sample holders for analysis using an X-ray diffractometer(XPERT-PRO, PAN analytical, Netherlands) to determine their crystal type (polymorph) and crystallinity. A slow scanning speed was selected ($1-2^{\circ}$ /min) for better resolution. According to (French, 2014), characteristic diffraction peaks for cellulose I β crystalline structure ($2\theta = 14.8^{\circ}$, 16.3° , 22.7°). The diffraction pattern was observed to determine the crystallinity index, as change in crystallinity confirms the incorporation of lignin enhances the mechanical properties and thermal stability of adsorbent. Diffractograms were recorded for both before and after adsorption. The index of crystallinity (CI) was calculated by Segal equation:

$$Cl(\%) = \frac{(I_{200} - I_{am})}{I_{200}} \times 100$$
 (3.2)

Where : I_{200} and I_{am} are the crystalline region and the amorphous region peak intensity, respectively.

3.2.3 Thermogravimetric Analysis (TGA)

The thermal stability and decomposition characteristics of raw CP, NC and LCNFs. For each analysis, a small, precisely weighed sample 10 mg was placed in a crucible within the TGA (SDT Q600 V20.9 Build 20 instrument (New Castle, USA). The samples were then heated over a defined temperature range, from ambient temperature 30 °C up to 800 °C, at a constant heating rate or 20 °C/min(Smith et al., 2020). This process was typically carried out under an inert atmosphere (nitrogen) with a consistent flow rate 20-50 mL/min to prevent oxidative degradation and isolate the thermal decomposition behavior of the materials. The instrument continuously monitored and recorded the weight loss of the sample as a function of increasing temperatures.

3.2.4 Point of zero charge (pHpzc) determination

The pH drift method was used to compute pHpzc. A series of solutions with varying pH values (2 to 10) was prepared using a background electrolyte NaCl (0.01 M). Ensuring the ionic strength of the electrolyte is consistent across all solutions. The pH of a 0.01M NaCl solution was changed to the desired pH by adding 0.01M hydrochloric acid or sodium hydroxide. A 2 g sample of LCNFs was added to each solution in separate containers. The containers were sealed to prevent contamination and changes in concentration due to evaporation. The containers were put on a shaker continuously for 24 hours to allow for equilibration. After

equilibration, the final pH of each solution was measured using a calibrated pH meter. The data was used to plot a graph to calculate the pHpzc, where the curve intersects the x-axis $(\Delta pH = 0)$.

3.2.5 Scanning Electron Microscopy (SEM-EDS) analysis

The surface morphology and topographical features of the synthesized LCNFs were investigated using SEM(Brno-Kohoutovice, Czech Republic). 10 mg of the dried LCNF sample was first mounted onto an aluminium stub using conductive double-sided carbon adhesive tape. Since the LCNFs materials are typically non-conductive, the mounted sample was subsequently sputter-coated with a thin, uniform layer of conductive material, typically gold or a gold-palladium alloy (~10-15 nm thickness), using a sputter coater machine to prevent charging effects and improve image resolution (Egerton, 2016). The prepared stub was then carefully loaded into the sample chamber of the scanning electron microscope. Images of the LCNF surface morphology were acquired at various magnifications under vacuum conditions, employing an accelerating voltage of 10 kV and utilizing the secondary electron (SE) detector for optimal topographical contrast (Goldstein et al., 2017). EDS(Brno-Kohoutovice, Czech Republic), integrated with SEM, allows for the identification and quantification of elements present in LCNFs.

3.2.6 Chemical composition

The chemical compositions of LCNFs were determined according to the method by (Ayeni et al., 2015)

3.2.6.1 Determination of ash content

First, the preheated crucibles were weighed and the weight recorded. Five samples of 2 g of LCNFs samples were put into five different crucibles and ignited on heating mantles until no more carbon fumes came out. The crucibles were transferred into the muffle furnace using metal tongs and ignited to carbon-free ash avoiding fusing. The crucibles were then removed after 3 hours and put in the desiccators to allow cooling. The samples were weighed to get the percentage of ash.

The ash % was calculated by the Equation 3.3:

$$Ash\% = \frac{\text{(sample weight after ashing)}}{\text{sample weight}}$$
(3.3)

3.2.6.2 Determination of moisture content

The preheated crucibles were weighed and the weight recorded. 5 samples of 2 g LCNF samples were inserted in pre-heated crucibles. The crucibles were sealed and subjected to heat in an oven drier with confined air circulation for 2 hours at 130 °C (Donato, 2016). The samples were then placed in a desiccator and cooled to room temperature before proceeding to weighing.

Moisture content, M_c was calculated by equation 3.4:

% Moisture =
$$\frac{M_i - M_{dried}}{M_i} \times 100$$
 (3.4)

Where:

M_i - initial mass

M_{dried} - final mass

3.3 Preparation of stock solutions

To investigate adsorption of ATA and TFV, individual stock solutions for both ATA and TFV were created using their respective commercially available tablets. For each drug, the tablet was crushed into a fine, uniform powder using a clean mortar and pestle, then transferred to a glass beaker and dissolved in deionized water and placed on a magnetic stirrer for 1 hour to ensure maximum dissolution of the active pharmaceutical ingredient. Since the tablets contained insoluble excipients, the resulting cloudy suspension was filtered by passing it through a 0.45 µm syringe filter to remove the visible particulate matter. The clearer filtrate, containing the dissolved drug, was transferred into a 1000 mL volumetric flask and diluted to the calibration mark with deionized water to yield a final stock solution with a concentration of 300 mg/L, which was then used to prepare all afterward experimental concentrations. The calibration curves were constructed after a series of standard solutions of decreasing concentrations were prepared by performing serial dilutions of the 300 mg/L stock solutions to determine the concentration of ATA and TFV in the polluted water samples based on their measured absorbance values.

3.4 Determination of the concentration of Atazanavir and Tenofovir

UV-Vis spectrophotometric measurements were performed using a UV-Vis (Thermo Scientific Genesys 10s,USA) spectrophotometer (Baird, 2017). The instrument was used to measure the

absorbance of standard solutions and polluted water samples at the wavelengths of maximum absorbance (λmax) for Atazanavir and Tenofovir.

3.5.0 Adsorption

Adsorption studies were carried out on a magnetic stirrer at 150 rpm in a 500 ml Erlenmeyer flask, 1 ± 0.02 g $- 3 \pm 0.02$ g of LCNFs was added to 100 ml of polluted sample. The processes were repeated 3 times on every variable and an average result was recorded as the final data obtained.

3.5.1 Effect of adsorbent dosage

The effect of LCNFs dosage on pollutant removal was studied by varying the mass of LCNFs added to the pollutant solution while keeping other parameters constant. Different masses of LCNFs from 1 ± 0.01 g to 3 ± 0.01 g were added to separate flasks each containing a fixed volume (100 ml) of the pollutant solution at a specific initial concentration of 300 mg/L, at optimal pH, and temperature at $40 \,^{\circ}$ C. The suspensions were agitated at $150 \,^{\circ}$ rpm for the predetermined equilibrium time $20 \,^{\circ}$ minutes (Wang et al., 2022). After equilibration, the LCNFs were separated from the solution by centrifugation, and the residual pollutant concentration was measured using UV-Vis(Thermo Scientific Genesys $10 \,^{\circ}$ s,USA) spectrophotometer to determine the removal efficiency and adsorption capacity at each dosage, thereby identifying the optimal or most effective adsorbent amount for the given conditions (Kumar et al., 2021).

3.5.2 Effect of pH

The effect of pH on the rate of adsorption of the LCNFs was evaluated by changing the parameter over the range of 2 - 10. The pH of the pollutant solutions (100 mL of 300 mg/L) was adjusted to the desired value using dilute solutions of 0.01 M NaOH and or 0.01 M HCl. 2 ± 0.02 g of LCNFs was added to the flask containing the contents were stirred at 150 rpm for the established equilibrium contact time. These experiments were conducted at a constant temperature of $25 \, ^{\circ}\text{C}$. Following adsorption, the mixture was centrifuged to separate the CNFs, and the final pollutant concentration was analyzed by the UV-Vis (Thermo Scientific Genesys 10 s,USA) spectrophotometer to evaluate the effect of pH on adsorption capacity and identify the optimal pH for maximum pollutant uptake, which provides insight into the potential adsorption mechanisms, such as electrostatic interactions (Zhang et al., 2022)

3.5.3 Effect of temperature

To evaluate the thermodynamic nature of the adsorption process, experiments were conducted at different temperatures, 20 °C to 60°C using a temperature-controlled shaker bath. For each temperature, a fixed mass of LCNFs (2 ± 0.02 g) was added to the pollutant solution 100 mL of 300 mg/L at the optimal initial pH (7). The mixtures were agitated at 150 rpm for the predetermined equilibrium time (20 minutes) (Wang et al., 2022). After equilibrium was attained, the LCNFs were separated by centrifugation and the residual pollutant concentration was measured by the UV-Vis (Thermo Scientific Genesys 10s,USA). The data obtained at different temperatures were used to calculate thermodynamic parameters such as Gibbs free energy change (ΔG°), enthalpy change (ΔH°), and entropy change (ΔS°) to understand the spontaneity and exothermic/endothermic nature of the adsorption.

3.5.4 Effect of contact time

To determine the time required to reach adsorption equilibrium, the effect of contact time was investigated by adding a fixed mass of 2.5 ± 0.02 g CNFs to a series of flasks containing the pollutant solution of 100 mL of 300 mg/L, at a constant initial pH and temperature. The flasks were agitated simultaneously at a constant speed of 150 rpm, and samples were withdrawn at predetermined time intervals from 20 to 140 minutes up to a point where no significant change in concentration was observed. Immediately after withdrawal, the CNFs were separated from the solution via centrifugation, and the residual pollutant concentration in the supernatant was analyzed by the UV-Vis (Thermo Scientific Genesys 10s,USA) to calculate the adsorption capacity (qt) at each time point, allowing the kinetic profile to be established.

3.6 Data treatment methods

3.6.1 Removal capacity and adsorption capacity

Adsorption capacity, Qe, was calculated using Equation 3.5:

$$Q_{e} = \frac{C_{i} - C_{f}}{m} x V \tag{3.5}$$

Where:

- C_i is initial drugs concentration
- C_f is final drugs concentration
- V is the volume of the solution
- *m* is the weight of the LCNFs

The removal capacity was calculated using Equation 3.6:

removal% =
$$\frac{C_i - C_f}{C_i}$$
 (3.6)

Where: C_i - is initial concentration and C_f - is final concentration.

3.6.2 Adsorption Isotherms

Langmuir and Freundlich's isotherms were used to calculate maximum adsorption capacity and intensity of ATA and TFV on LCNFs.

For Langmuir isotherm Equation (3.7) was used:

$$\frac{C_{\rm e}}{Q_{\rm e}} = \frac{1}{QK} + \frac{C_{\rm e}}{Q} \tag{3.7}$$

Where:

Qe is the equilibrium adsorption capacity

C_e is the equilibrium concentration.

K₁ is the Langmuir constant related to the binding sites

Q_m/Q is the maximum adsorption capacity

For Freundlich isotherm, Equations 3.8 and 3.9 were used:

$$Q_e = K_f C_e^{\frac{1}{n}} \tag{3.8}$$

$$lnQ_e = lnK + \frac{1}{n} lnC_e$$
 (3.9)

Where:

Qe is the equilibrium adsorption capacity

C_e is the equilibrium concentration.

K is the Freundlich constant related to the adsorption capacity. $\frac{1}{n}$ is the Freundlich constant related to adsorption intensity.

3.6.3 Adsorption kinetics

The pseudo-first order (Equation 3.10) and pseudo-second order (Equation 3.11) were used to determine the adsorption kinetics (Ruziwa et al., 2015).

$$In(Q_t - Q_e) = InQe + K_1 t$$
(3.10)

$$\frac{t}{Q_t} = \frac{1}{K_2 Q_e^2} + \frac{1}{Q_e} \tag{3.11}$$

Where $Q_e(mg/g)$ and $Q_t(mg/g)$ are adsorption capacities at equilibrium and at time t, respectively k_1 (L/min) is the pseudo-first order rate constant and k_2 (g/mg/min) is the pseudo-order rate constant.

3.6.4 Thermodynamics

The effect of solution temperature was evaluated using the van't Hoff equation (Equation 3.12) to determine the enthalpy change and entropy change for the process of adsorption. To calculate the Gibb's free energy change of adsorption, the Gibbs equation (Equation 3.13) was used (Chaukura et al., 2016).

$$\ln\left(\frac{\text{Qe}}{\text{Ce}}\right) - \frac{\Delta H}{\text{RT}} + \frac{\Delta S}{R} \tag{3.12}$$

$$\Delta G = -RTIn(\frac{Qe}{Ge})$$
 (3.13)

Where:

R (8.314 J/mol/K) is the universal gas constant, T (K) is the absolute solution temperature.

CHAPTER 4: RESULTS AND DISCUSSION

In this chapter, the results of the adsorption studies are analyzed and discussed. The characteristics of Raw CP, NC and LCNFs are also evaluated. The implications of these findings on and after the adsorption process are thoroughly examined.

4.1 Percentage yield and purity

The yield and purity analysis from 100 g of raw CP revealed distinct differences between LCNFs and the nanocellulose before fibrillation. LCNFs demonstrated a yield of 49.5 ± 0.9 % due to some mass loss during the fibrillation process and the washing stages involved, while nanocellulose showed a higher yield of 60 ± 0.4 %, likely due to less intensive purification steps that preserved more cellulose. However, LCNFs achieved greater purity (80 ± 0.2 %) compared to nanocellulose (70 ± 0.3 %), resulting from more effective removal of noncellulosic components whilst retaining lignin as shown in (Table 4.1). The superior purity of LCNFs indicated better-defined surface chemistry, which is crucial for adsorption applications. These yield percentages are because of a significant amount of cellulose lost during the repeated washing stages that were done until the desired neutral pH was reached.

4.2 Characteristics of raw Cassava Peel (CP), Nanocellulose (NC) and Synthesized adsorbent

4.2.1 Physico-chemical characteristics of raw CP and synthesized adsorbent

Raw CP and its processed forms NC and LCNFs were analyzed, with important implications for their adsorption capabilities as shown in (Table 4.1). The pH_pzc increased from 3.2 ± 0.2 (Raw CP) to 4.5 ± 0.3 (LCNFs), this indicated a significant modification of the surface functional groups during processing. Such an increase in pH_pzc is attributed to the removal of highly acidic components, like hemicelluloses, during the chemical and mechanical treatment, which results in a less acidic, or more basic, surface overall (Chen et al., 2020) . The moisture content was reduced from 20.5 ± 1.4 %, to 8 ± 1.4 %, indicating improved stability, while the significant decrease in ash content from 5.6 ± 0.4 % to 0.6 ± 0.1 % confirmed the effective removal of inorganic impurities during the alkali, bleaching and washing stages that could have blocked reactive sites(Adelodun et al., 2021).

Significantly, the lignin content was reduced but largely retained, whilst hemicellulose was almost entirely removed during the bleaching stage. This selective removal of hemicellulose is a key strategy for enhancing the accessibility to the core cellulose structure and its functional

groups (Chen et al., 2020). The retained lignin provides crucial hydrophobic and π - π interaction sites from its aromatic rings, while the now-exposed hydroxyl (-OH) groups on the cellulose, along with carboxyl (-COOH) groups introduced during processing, serve as primary reactive sites for hydrogen bonding and electrostatic interactions with drug molecules (Bian et al., 2021). The pH_{pzc} indicated that LCNFs have a more neutral surface charge, which is beneficial for adsorbing both cationic and anionic drugs at different pH levels.

Table 4.1: Comparison of raw CP, anocellulose and LCNFs

	Raw CP	Nanocellulose	LCNFs
pHpzc (%)	3.2 ± 0.2	4.0 ± 0.2	4.5 ± 0.3
Moisture content (%)	20.5 ± 1.4	8.4 ± 1.4	8.0 ± 1.3
Ash content (%)	5.6 ± 0.4	0.8 ± 0.1	0.6 ± 0.1
Lignin (%)	15.5 ± 0.6	7.5 ± 0.5	7.5 ± 0.4

4.2.2 Surface morphology and elemental composition

The heterogeneity and porous structure of the materials before and after bio-sorption were observed in the SEM micrographs.

4.2.2.1 Cassava Peel (CP)

The SEM results for Raw CP (Figure 4.1) shows a heterogeneous surface characterized by relatively large, irregular particles, typically tens of micrometres in size, with smaller particulate matter interspersed among them. Its texture appeared rough, and visible interstitial spaces between particles indicated a degree of macroporosity. Compared to its processed nanoforms, the raw peel possessed a relatively lower specific surface area, and any intrinsic microporosity within its lignocellulosic structure was generally less accessible, these observations are consistent with previous characterizations of raw cassava peel (Adelodun et al., 2021).

The EDS showed its elemental composition, carbon (C) and oxygen (O) being the most dominant elements, at 50.5 Wt% and 46.8 Wt% respectively, which is expected for organic biomass material primarily composed of carbohydrates like cellulose (Putra et al., 2022). Minor inorganic elements detected include potassium (K, 1.4 Wt%), calcium (Ca, 0.5 Wt%), silicon

(Si, 0.4 Wt%), copper (Cu, 0.3 Wt%), and magnesium (Mg, 0.2 Wt%), indicating the presence of trace minerals or salts within the peel (Figure 4.1).

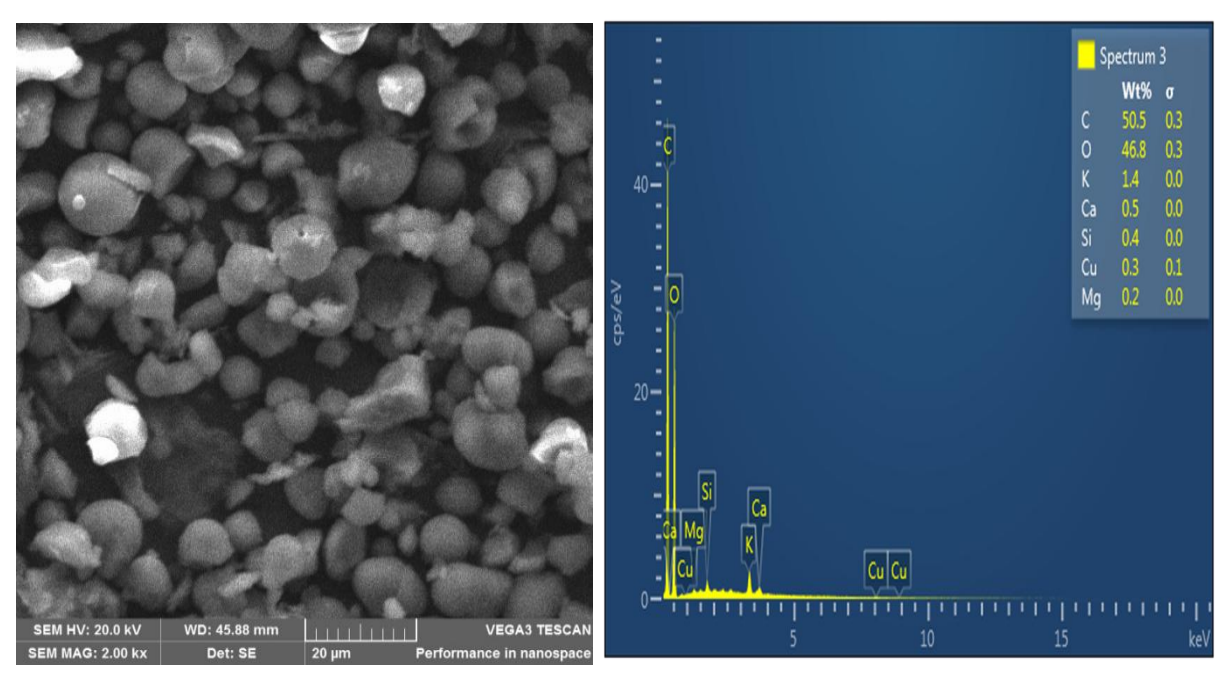


Figure 4.1 : SEM micrograph (left) and corresponding SEM-EDX (right) for raw CP

4.2.2.2 Nanocellulose (NC)

SEM revealed significantly increased surface area and porosity with multi pore developing (Figure 4.2) compared to raw peel, with more binding sites getting exposed due to its layered, flaky and networked structure with numerous crevices and edges observed (Figure 4.2).

The EDS(Figure 4.2) analysis of the nanocellulose revealed high weight percentages of (C, 55.3 Wt%) and (O, 42.0 Wt%), consistent with its cellulosic nature rich in hydroxyl (-OH) and carboxyl groups(Putra et al., 2022). Trace inorganic elements such as calcium (Ca, 1.7 Wt%), iron (Fe, 0.4 Wt%), phosphorus (P, 0.3 Wt%), and silicon (Si, 0.2 Wt%) were also detected, which may have arisen from impurities or deionized used during the extensive washing and processing stages. These results confirmed the primarily organic composition of the nanocellulose, with minor inorganic residues which is consistent with similar studies on nanocellulose derived from cassava biomass (Olawale et al., 2021).

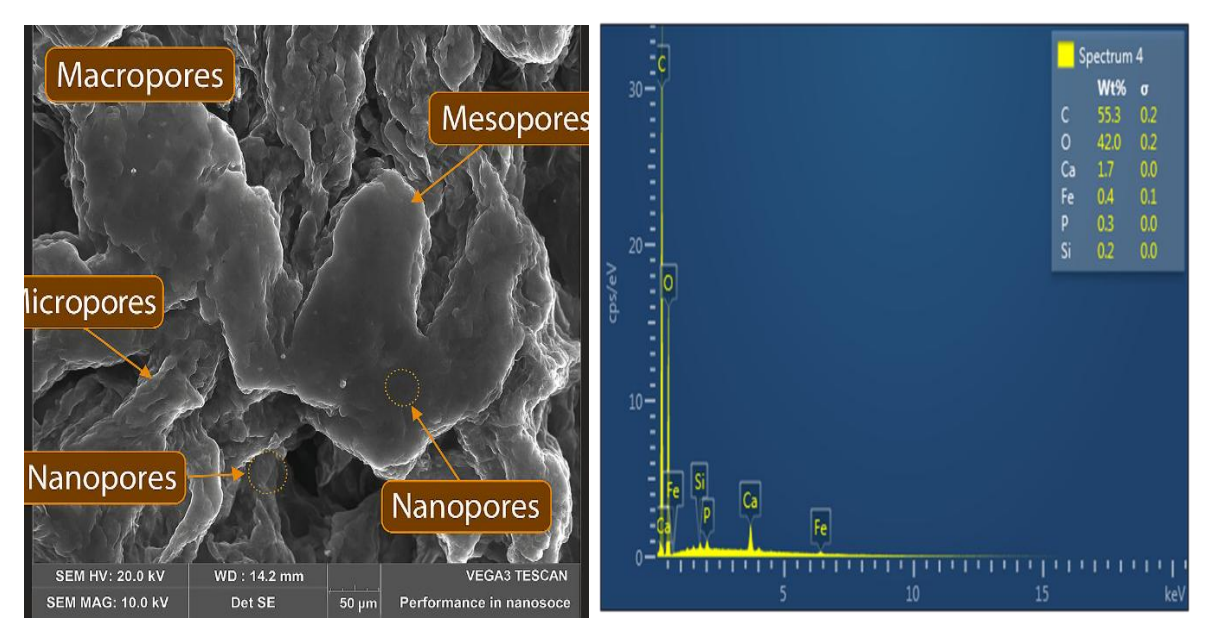


Figure 4.2 : SEM micrograph (left) and corresponding SEM-EDX (right) for NC

4.2.2.3 Lignin Cellulose Nanofibrils (LCNFs)

Possessed a markedly higher specific surface area and more developed hierarchical porosity with a multitude of interstitial voids, including mesopores, micropores and macropores (Figure 4.3) compared to the CP and NC due to fibrillation. The observed layered and flaky nature, along with numerous crevices and edges, through the complex three-dimensional arrangement of an agglomerated fibrillar structures directly contributed to this increased surface area. The irregular structure observed is due to the retention of the amorphous region (lignin). These crevices, rough surface, and edges (Figure 4.3) not only increased the surface area but also acted as active sites for drug adsorption, leading to higher potential loading capacity therefore increasing adsorption capacity (Bian et al., 2021).

The EDS(Figure 4.3) spectrum for the LCNFs indicated a predominant composition of C at 54.5 Wt% and oxygen O at 45.3 Wt%, reflecting the organic cellulosic structure rich in hydroxyl & carboxyl groups which contributed to the hydrogen bonding with the adsorbates. A trace amount of calcium (Ca) was also detected at 0.3 Wt%, which could be an inherent to the original cellulose source. These results primarily confirmed the high purity of the organic LCNFs, which is a key characteristic of this class of functional materials (Zhao et al., 2020).

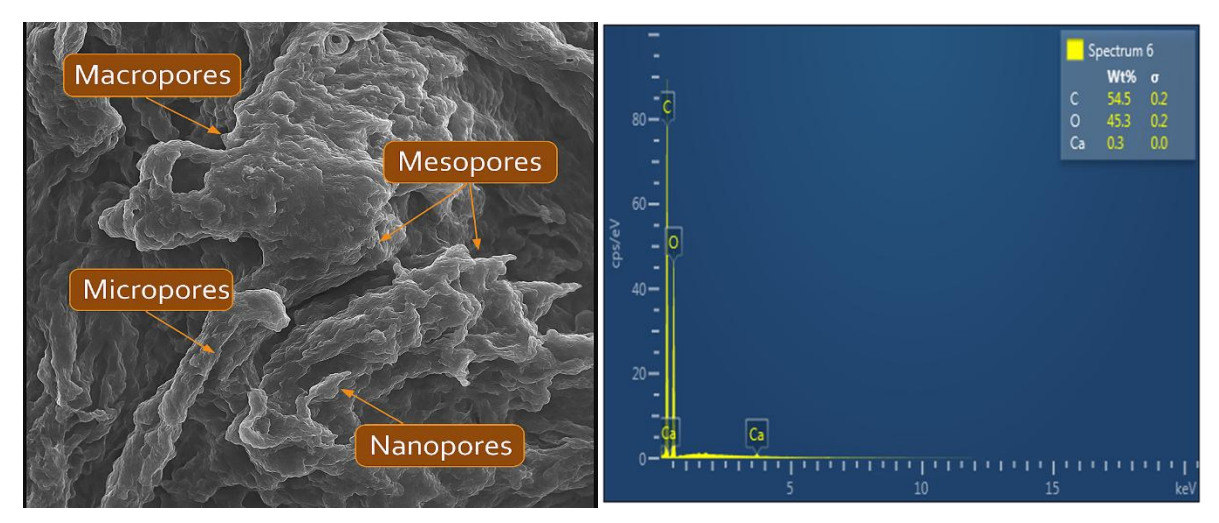


Figure 4.3: SEM micrograph (left) and corresponding SEM-EDX (right) for LCNFs

4.2.2.4 Before and After Adsorption Scanning Electron Microscopy (SEM) Comparison

The observed multi-porosity and structural heterogeneity before adsorption in Figure (4.4, 4.5 & 4.6) are common in many adsorbent materials and are crucial for providing active sites for adsorption (Thommes et al., 2015). The multi pores, irregular surfaces and crevices explains the favourable adsorption kinetics observed, as the extensive surface area provides numerous binding sites for ATA and TFV molecules. In contrast, the right image (after adsorption) in Figure 4.6 shows a more combined morphology with reduced pore visibility and smoother surfaces, indicating significant surface coverage by the adsorbed pharmaceuticals (Wang et al., 2022). The partial filling of pores and blurring of fibril boundaries suggest that drug molecules not only coat the surface (Figure 4.5 right image) but may also penetrate the nanofibril network, causing structural rearrangements to accommodate the adsorbates (Zhou et al., 2023).

The observed morphological changes align well with the thermodynamic and kinetic data. The surface coverage and pore filling visible in the post-adsorption image support the chemisorption mechanism suggested by the PSO model, as such extensive surface interactions would require strong adsorbate-adsorbent bonding (Ahmed et al., 2021). The structural stabilization also helps explain the endothermic nature of the process ($\Delta H^{\circ} > 0$), as energy would be required for both the dehydration of surfaces and the conformational changes in the nanofibril matrix (Xu et al., 2022). The maintenance of the overall fibrous structure after adsorption(Figure 4.5) indicates good structural stability of the adsorbent, suggesting potential for regeneration and reuse in water treatment applications (Chen et al., 2023). These SEM observations, combined with the kinetic and thermodynamic data, provide a comprehensive

analysis of the sorption process, from molecular interactions to macroscopic morphological changes.

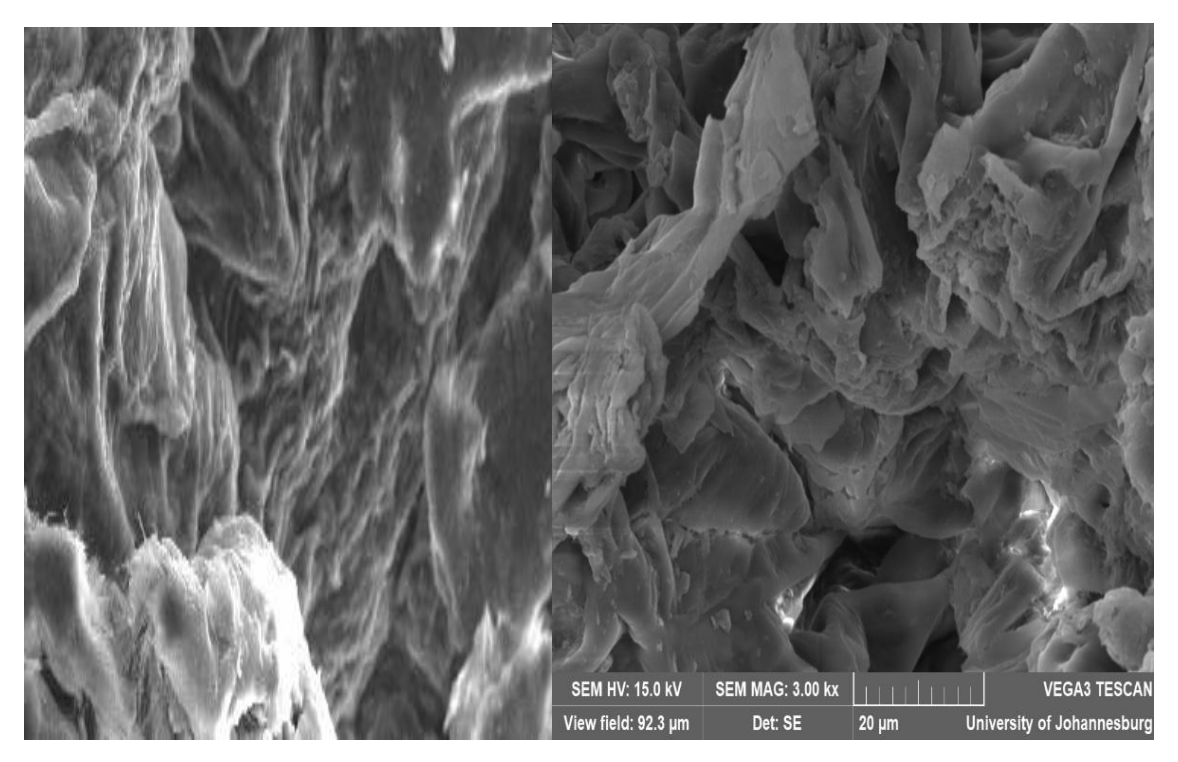


Figure 4.4 : SEM micrographs at 20μm, Before(left) & After (right) adsorption

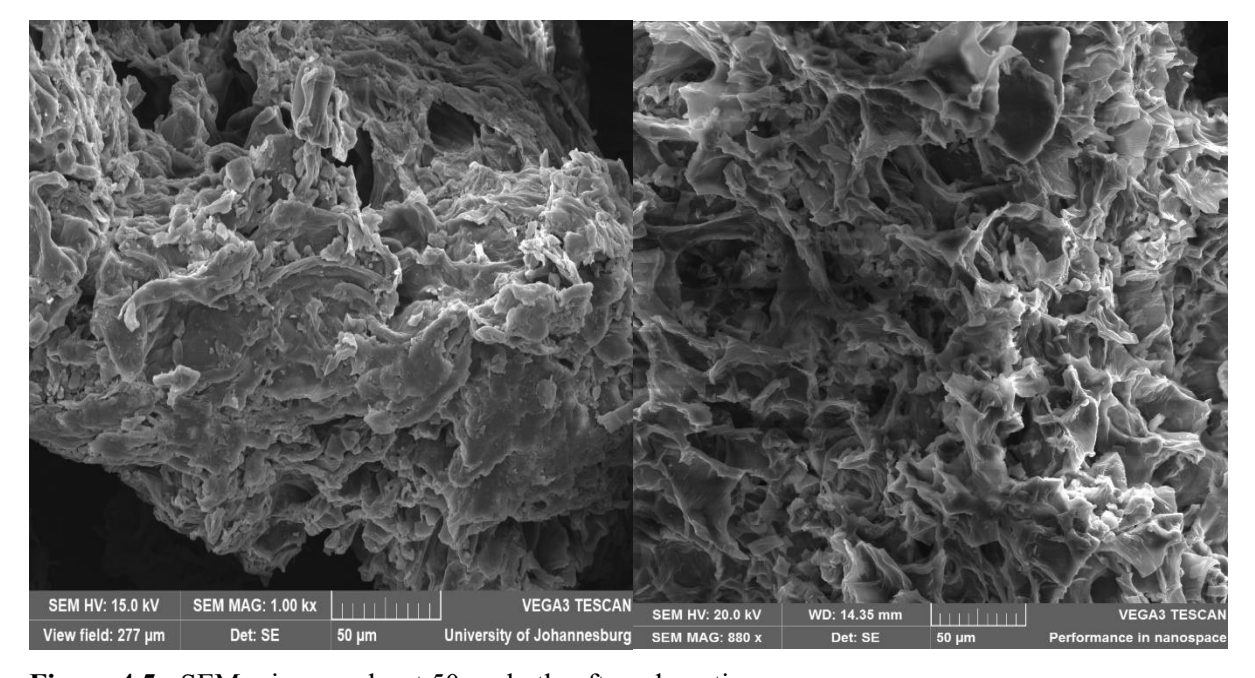


Figure 4.5 : SEM micrographs at 50μm both after adsorption

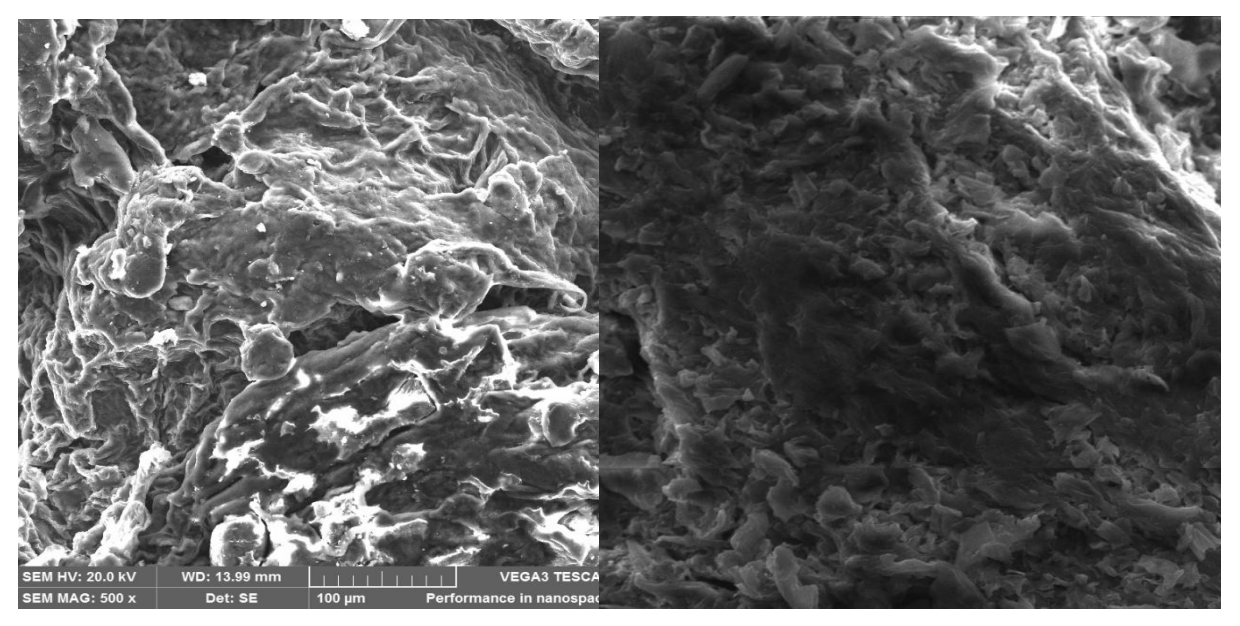


Figure 4.6: SEM micrographs at 100 µm, Before(left) & After (right) Adsorption

4.2.3 Thermogravimetric Analysis (TGA)

The raw CP initiated degradation at the lowest temperature range, observed 200-250°C. This early decomposition was characteristic of lignocellulosic biomass where less thermally stable components, primarily hemicellulose, degraded first (Özsin and Pütün, 2019). NC exhibited enhanced thermal stability compared to raw CP, sharp decomposition phase occurred at higher temperatures 275°C and 400°C. This behavior was typical for purified cellulosic materials, where increased crystallinity and the removal of other components led to a more defined and higher-temperature degradation profile(Pereira et al., 2020). LCNFs demonstrated the most pronounced weight loss among the three samples in the 250°C to 500°C range(Figure 4.7). The presence of lignin, with its wider decomposition range, contributed to this broader degradation profile (Abdel-Karim et al., 2022).

At elevated temperatures (>600°C), the raw CP curve indicated the highest residual mass. This was consistent with the presence of thermally resistant lignin, known for higher char yield, and inorganic ash in raw biomass (Gaurav et al., 2023). NC left a moderate char yield. LCNF, containing lesser lignin, resulted in a final residue lowest and comparable to NC. Interactions between cellulose and lignin at the nanoscale in LCNFs could lead to complex degradation pathways (Bian et al., 2017).

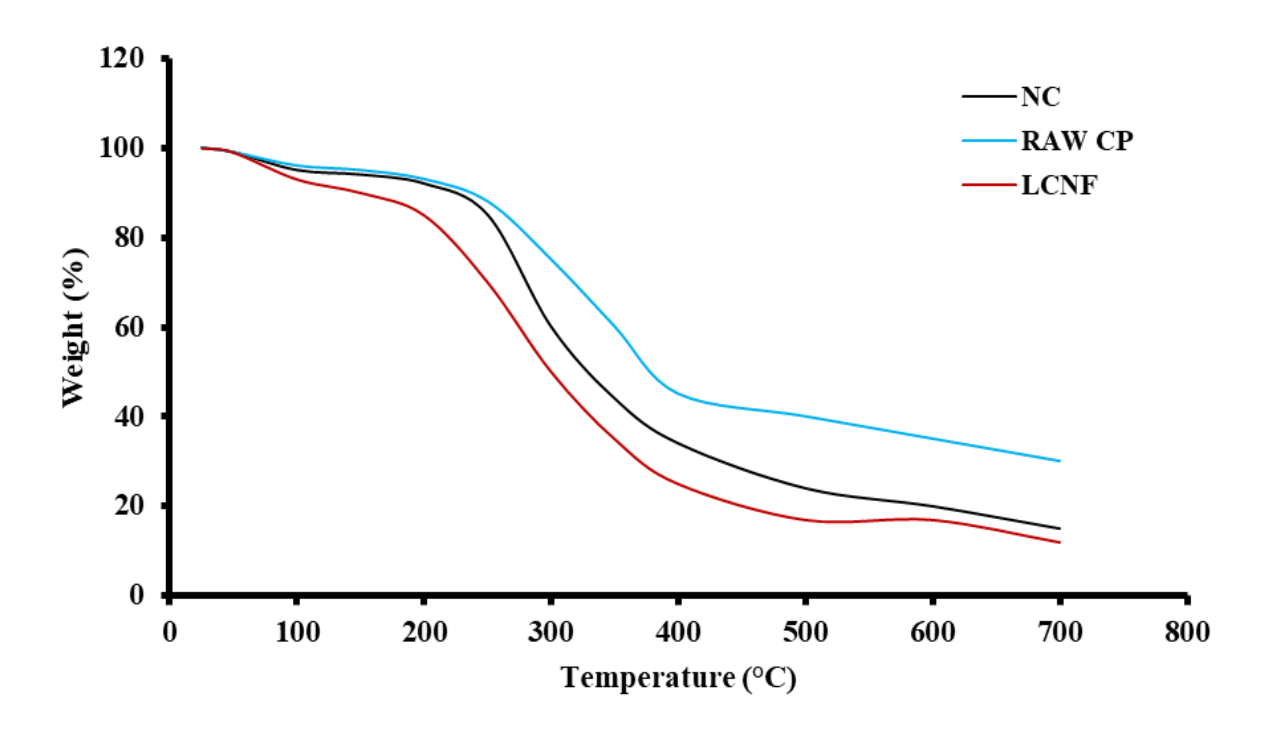


Figure 4.7: TGA thermograms for raw CP, NC & LCNFs

4.2.4 Fourier Transform Infrared Spectroscopy Analysis (FTIR)

The FTIR spectra of CP, NC, and LCNFs were analyzed to observe the chemical changes occurring during the synthesis stages (Figure 4.8). All three samples displayed characteristic peaks for lignocellulosic materials, including a broad hydroxyl (-OH) stretching band around 3400 cm⁻¹ and a C-H stretching peak near 2900 cm⁻¹ and a key transformation observed was the significant reduction of the peak around 1730 cm⁻¹, attributed to the C=O stretching in hemicellulose, in both the NC and LCNFs spectra, confirming the successful removal of hemicellulose(Das et al., 2024; Rasheed et al., 2023). Significantly, the peak at approximately 1515 cm⁻¹, which is characteristic of aromatic skeletal vibrations in lignin, is clearly present in the raw CP and is retained in the LCNFs but is diminished in the NC sample. This confirms the successful production of a lignin-containing nanofibrils. The LCNFs adsorbent therefore possessed pre-dominant hydroxyl groups from cellulose and accessible aromatic rings from lignin, creating a rich surface chemistry with multiple active sites for potential drug interactions.

Following the batch adsorption experiments for the two drugs, the adsorbent samples used for Atazanavir (LCNFs1) and Tenofovir (LCNFs2) were analyzed to confirm the successful biosorption of the drugs (Figure 4.8). In the spectrum for LCNFs2, the most compelling evidence for Tenofovir adsorption is the appearance of new peaks in the 1100-950 cm⁻¹ region, which are assigned to the P-O and P=O stretching vibrations from the phosphonate group of the

Tenofovir molecule (Ncibi & Sillanpää, 2018). For LCNFs1, the successful adsorption of Atazanavir is indicated by subtle but significant changes in the 1700-1500 cm⁻¹ region, including a slight broadening and increase in intensity around 1650 cm⁻¹ and 1580 cm⁻¹, corresponding to the C=O stretching of amide groups and N-H bending vibrations from the drug (Gao et al., 2021). Furthermore, the broad -OH band around 3400 cm⁻¹ in both LCNFs1 and LCNFs2 appears broader and slightly shifted compared to the original LCNF spectrum, suggesting that the hydroxyl groups on the adsorbent surface are actively involved in hydrogen bonding with both drug molecules(Hokkanen et al., 2016). These distinct spectral changes provided strong evidence that the physical changes observed in the XRD analysis, where the strong surface binding is significant enough to induce lattice strain and cause a broadening of the cellulose diffraction peaks.

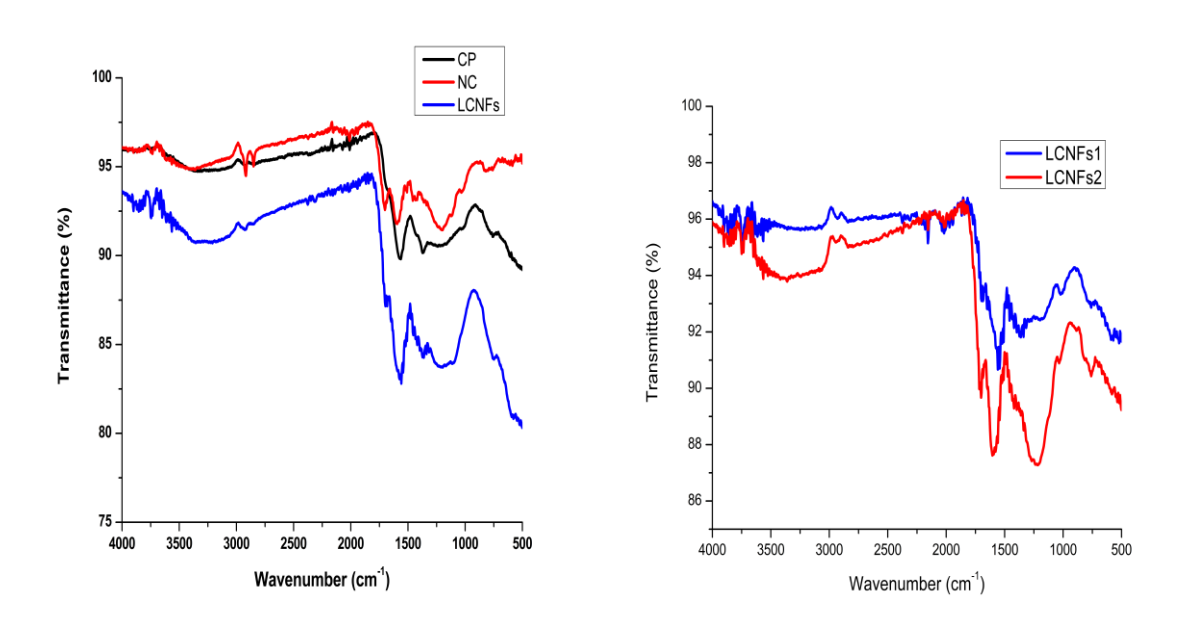


Figure 4.8 :FTIR Spectra of raw CP, NC and LCNFs (left) before sorption and (right) after sorption of ATA using LCNFs1 and TFV using LCNFs2

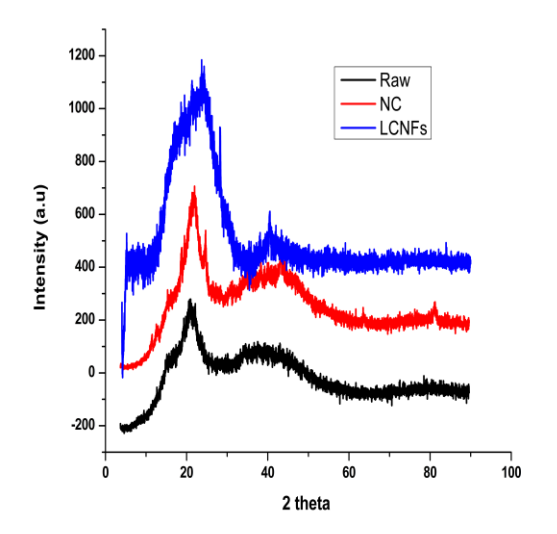
4.2.5 X-ray diffraction Analysis (XRD)

XRD analysis was performed to evaluate the changes in crystallinity of the materials from the raw state through synthesis(figure 4.9). The diffractogram for the raw CP displayed a broad, low-intensity peak centred at $2\theta = 22^{\circ}$, indicative of a semi-crystalline structure with a high proportion of amorphous content. Following the chemical and mechanical treatments, both the NC and the LCNFs exhibited much sharper and more defined diffraction peaks. The characteristic peaks for the cellulose I β crystal structure are clearly visible at $2\theta \approx 16.3^{\circ}$ and 22.7° (Khadraoui et al., 2022). This significant increase in peak intensity and sharpness corresponds to a higher Crystallinity Index (CrI), confirming the effective removal of

amorphous components the hemicellulose during processing (Nam et al., 2016). The high crystallinity of the final LCNF adsorbent is a desirable characteristic, suggesting robust structure suitable for use as a stable adsorbent.

The structural integrity of the adsorbent after the adsorption of Atazanavir (LCNFs1) and Tenofovir (LCNFs2) was assessed by comparing their XRD patterns to the before sorption LCNF diffractogram, the primary diffraction peaks of cellulose I β at ~16° and ~22.7° were preserved in both the LCNFs1 and LCNFs2 spectra. This demonstrated that the fundamental crystalline backbone of the adsorbent was not disrupted, indicating excellent structural stability during the adsorption process, the sorption happened through interactions with the available functional groups (-OH, -COOH, lignin sites) on the solid.

However, significant broadening of the main crystalline peak at \sim 22.7° was observed in both LCNFs1 and LCNFs2 compared to the original LCNFs sample which suggested a strong, intimate interaction between the drug molecules and the adsorbent, which induces minor strain or disorder on the surface layers of the cellulose crystal lattice (Li et al., 2020). In addition to the main cellulose peaks, both spectra exhibit a distinct, sharp diffraction peak at approximately $20 \approx 32.5^{\circ}$, these narrow peaks, which are not characteristic of the adsorbent appeared after contact with the drugs, showing a characteristic diffraction peak from a small fraction of the drug molecules that have crystallized on the adsorbent surface, the absence of other major drug peaks suggests the majority of the adsorbed molecules are likely distributed in the noncrystalline (amorphous) state (Liu et al., 2021). The overall retained structure is a positive indicator of the adsorbent's robustness, showing its potential for regeneration and reuse in practical applications (Chen et al., 2023). The crystallinity index calculated from the Segal equation showed that crystallinity increased from 30% (raw CP) to 72% (LCNFs) whilst NC had the highest 80%. LCNFs1 and LCNFs2 returned almost the same crystallinity 70% and 71% respectively, after adsorption confirming their structural stability.



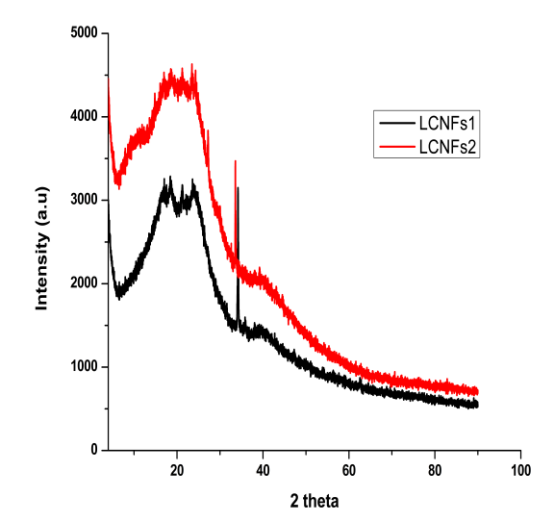


Figure 4.9: XRD diffractograms of raw CP, NC and LCNFs before (left) and after (right) adsorption of ATA using LCNFs1 and TFV using LCNFs2

4.3 Effects of Experimental Conditions

The efficiency of ATA and TFV removal by LCNFs was evaluated using UV-Vis Spectroscopy by varying key experimental parameters(Figure 4.10) during the batch adsorption experiments. Understanding the influence of these conditions was crucial for optimizing the adsorption process and elucidating the underlying removal mechanisms.

4.3.1 Adsorbent dosage

The data obtained showed a significant increase in removal efficiency as the dosage was raised from 0.5 g, reaching peaks of 95% (ATA) and 93% (TFV) removal for both drugs at a dosage of 2.5 g. Beyond this, the removal efficiency showed little to no further increase, and even a slight decrease to 90% at 3.0 g(Figure 4.10 (a)). This is a trend where an initial increase in removal is attributed to a greater availability of active binding sites and a larger surface area. However, a plateau or slight decrease at higher dosages can occur due to the saturation of adsorbate molecules or the aggregation of adsorbent particles, which reduces the effective surface area per unit mass (Bayo, 2021; Anbia and Ghaffarinejad, 2015). Such optimal dosage effects, beyond which minimal improvement is observed, are frequently reported for cellulose nanofibril-based adsorbents in pollutant removal (Mishra and Tiwari, 2021).

4.3.2 Temperature

Temperature exerted a notable influence on the removal process, with the percent removal for both ATA and TFV increasing as the temperature rose from 10°C to an optimum of approximately 40°C, where removal efficiencies of TFV(94%) and ATA (93%) were achieved.

A further increase in temperature to 50°C led to a slight decrease in removal for ATA (92%) & (93%)TFV(Figure 4.10 (d)). The trend of the results obtained for ATA and TFV show evidence that percentage removal increases as temperature increases because of the increase in mobility of the adsorbed species and an increase in active sites. This behavior often suggests that the adsorption process is initially endothermic, favoured by an increase in temperature which can enhance the kinetic energy and diffusion rate of drug molecules (Wang et al., 2019). The slight decline at higher temperatures might indicate that the process becomes less favourable, possibly due to the exothermic nature of certain physisorption interactions(hydrogen bonding) becoming dominant, or potential alterations in adsorbent stability or increased desorption tendencies at elevated temperatures (Al-Ghouti & Da'ana, 2020).

4.3.3 pH

The solution pH demonstrated distinct effects on the removal of ATA and TFV, highlighting the importance of surface chemistry and drug speciation. For ATA, removal efficiency increased with pH from 2, peaking at 90-92% within the pH range of 5 to 6, after which it declined to 78% at pH 10(figure 4.10 (b)). However, TFV showed a continuous increase in removal with rising pH, achieving 90% removal at pH 8 and maintaining a similar high efficiency of 88-90% at pH 10. Such pH-sensitive behavior is primarily influenced by pH on the surface charge of the lignin-containing cellulose nanofibrils (through protonation/deprotonation of hydroxyl and carboxyl groups) and the ionization state of the drug molecules, which dictates the nature and strength of electrostatic interactions and other binding mechanisms (Agustin et al., 2022: Szymański et al., 2020). The differing optimal pH ranges underscore that specific pH conditions are required to maximize the attractive forces between each drug and the adsorbent surface(Szymański et al., 2020).

4.3.4 Contact Time

Contact time played a crucial role in the adsorption process, with the percent removal for both ATA and TFV rapidly increasing during the initial phase and then gradually slowing to reach a near-equilibrium state. Optimal removal, achieving 90-94% for ATA and 90-93% for TFV, was observed around 120-140 minutes(Figure 4.10 (c)). This kinetic profile is characteristic of adsorption processes, where the initial fast uptake is driven by the abundant availability of active sites on the adsorbent surface. As these sites become progressively occupied, the adsorption rate decreases until equilibrium is established (Tran et al., 2017). The time required to reach this equilibrium is an important parameter for designing efficient adsorption systems

and is consistent with findings for various pharmaceutical compounds on lignocellulosic and nano cellulosic adsorbents (Nasrullah et al., 2019).

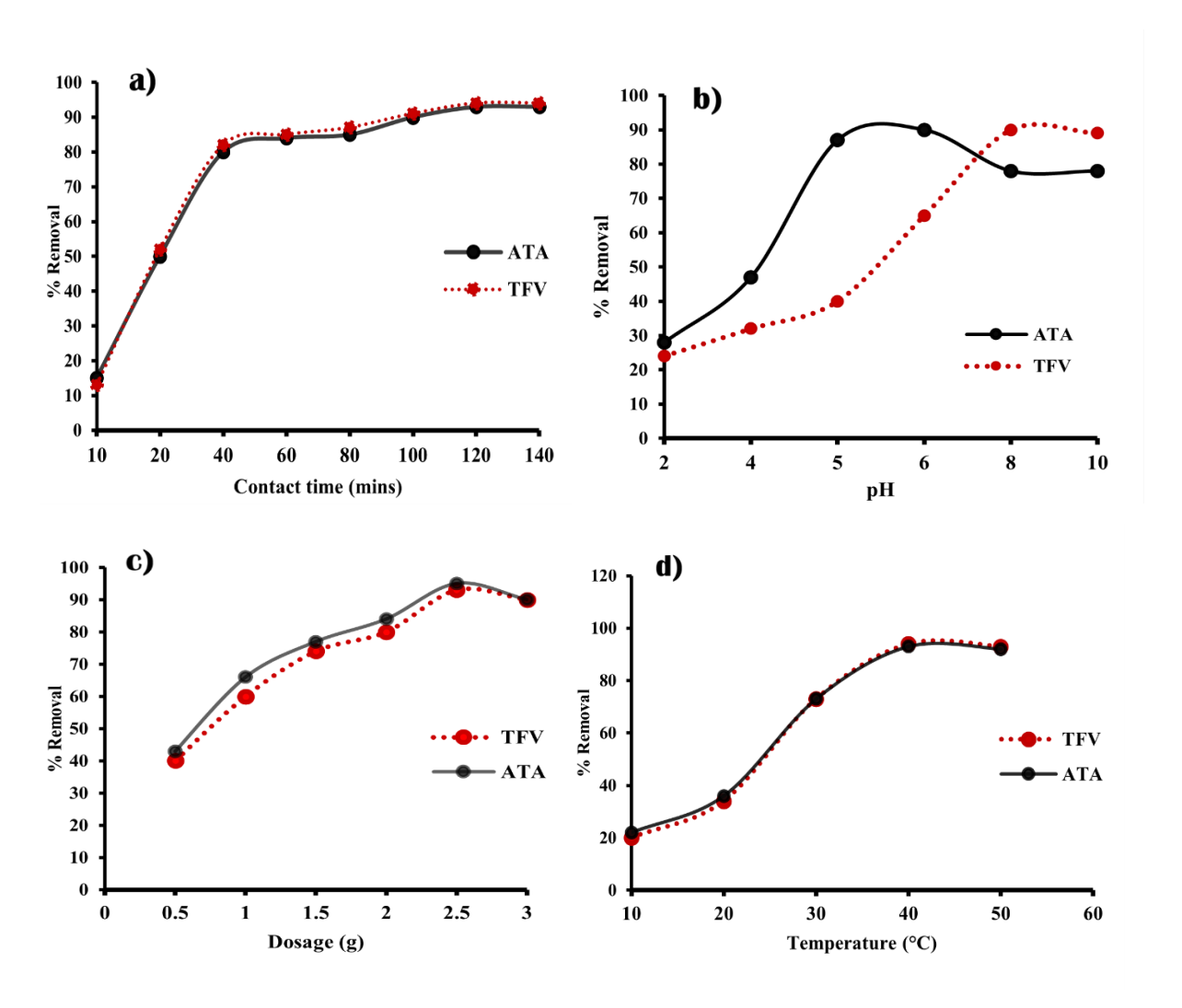


Figure 4.10: Experimental conditions: effect of contact time (a), effect of pH (b), effect of dosage (c) and effect of temperature (d)

4.4 Isothermic modelling

The comparison of the correlation coefficients (R^2) showed that the freundlich model provided a significantly better fit for the experimental data for both ATA ($R^2 = 0.9681$) and TFV ($R^2 = 0.9843$) compared to the Langmuir model, ATA ($R^2 = 0.9115$) and TFV ($R^2 = 0.8564$). This indicated that the Freundlich isotherm is the more suitable model to describe the equilibrium behavior of this system. The strong fit suggested that the adsorption occurs on a heterogeneous surface in multiple layers, which is characteristic of complex biosorbents like LCNFs (Al-Ghouti & Da'ana, 2020). The high Freundlich intensity factors, n, of 1.68 for ATA and 1.40 for TFV, confirmed that the process was highly favourable. The adsorption processes with n greater than 1 is evidence of a favourable adsorption process (Chaukura et al.,2017).

The strong chemical affinity was reflected in the respectable adsorption capacity constants, K_f of 11.15 and 9.97 (mg/g)(L/mg)^{1/n} for ATA and TFV, respectively. Whilst the Freundlich model provided the best description, the parameters from the langmuir model serve as a useful performance benchmark. The calculated maximum adsorption capacities (q_{max}) of 84.22 mg/g for ATA and 80.42 mg/g for TFV established the synthesized LCNFs as a high-capacity adsorbent, competitive with other advanced nanocellulose-based materials (Kalia & Gola, 2022).

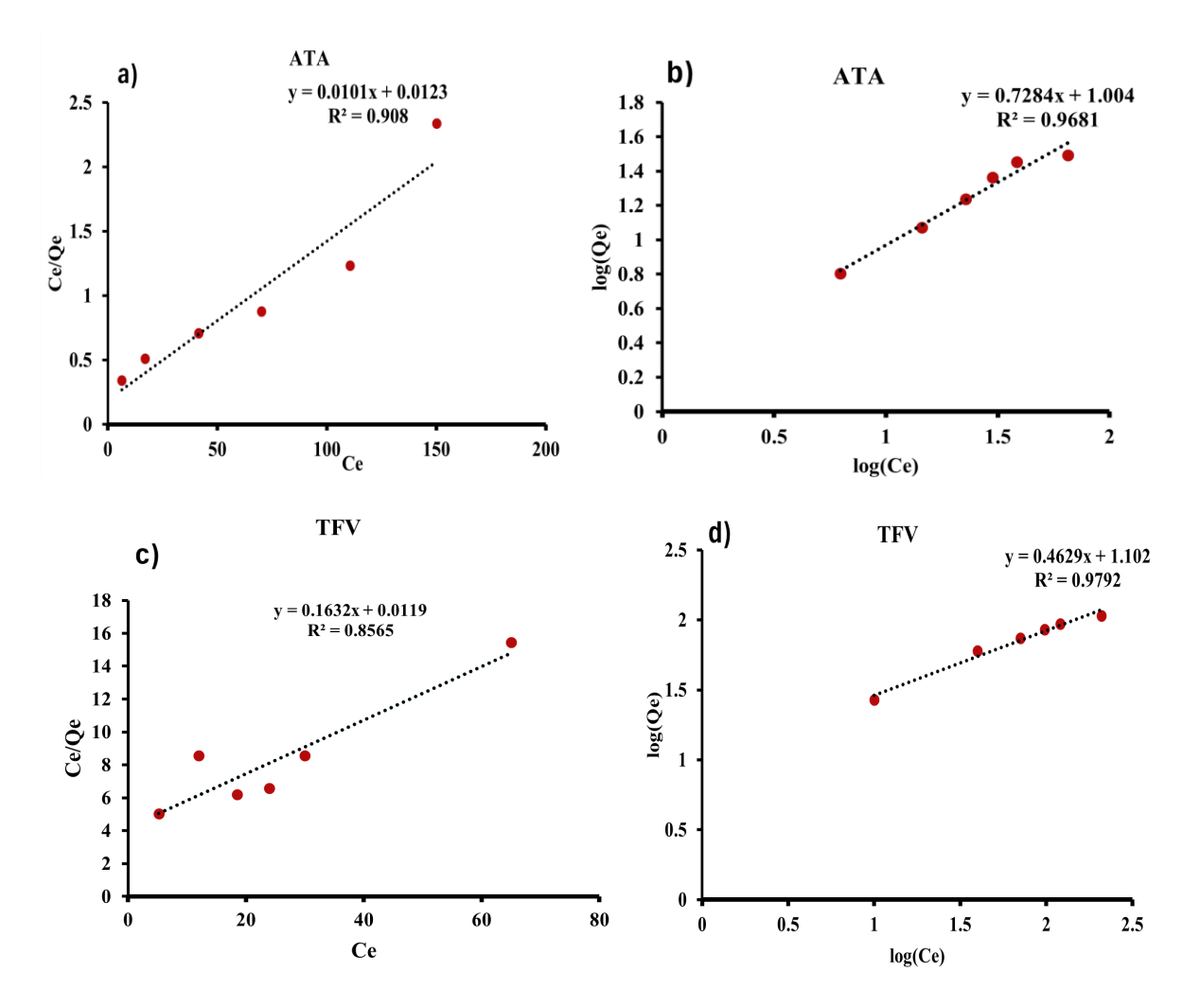


Figure 4.11: Langmuir model for the adsorption of ATA (a), Freundlich model for the adsorption of ATA (b), Langmuir model for the adsorption of TFV (c) and Freundlich model for the adsorption of TFV (d)

4.5 Adsorption Kinetics

To understand the adsorption mechanism further pseudo-first-order (PFO) and pseudo-second-order(PSO) models were analyzed. These helped determine whether adsorption is between physical adsorption (PFO, involves diffusion-controlled processes) and chemisorption (PSO,

involving chemical interactions between adsorbate and adsorbent) (Tran et al., 2020; Ayawei et al., 2017).

PFO for ATA obtained rate constant (k_1) of 0.015 min⁻¹ and predicted q_e of 8.037 mg/g (R^2 = 0.9477) (Figure 4.10), suggesting some involvement of physical adsorption processes. While the PFO provided a reasonable fit, the deviation in later stages (evident from the declining linearity at higher time points) suggests that physical diffusion alone cannot fully describe the adsorption process. Hence, the PSO ($R^2 = 0.9818$) with a calculated q_e of 91.20 mg/g clearly indicates that chemisorption dominates the adsorption mechanism. This is consistent with recent studies showing that lignin-containing adsorbents frequently exhibit PSO kinetics due to their abundant functional groups that facilitate chemical interactions with pharmaceutical compounds (Jawad et al., 2020). The significant difference between the PSO qe and the PFO qe contributed to the complex porous structure of LCNFs, which can create diffusion limitations not fully captured by simple kinetic models (Largitte and Pasquier, 2016). The moderate PSO (k₂ = 0.015 g/mg·min) obtained is characteristic of lignocellulosic materials, reflecting their balanced combination of surface functional groups and porous structure (Thue et al., 2018). The higher q_e by PSO compared to Langmuir Q_m mg/g) suggests the potential formation of multilayers or the involvement of multiple adsorption sites, on biomass-derived materials (Bonilla-Petriciolet et al., 2019).

The PFO for TFV showed (R² = 0.9863)(Figure 4.10) with (k₁) of 0.0191 min⁻¹ and (qe) of 11.27 mg/g calculated from the intercept value. This strong correlation suggests that physical adsorption processes, potentially including pore diffusion and weak intermolecular forces, contribute significantly to TFV uptake (Largitte and Pasquier, 2016). However, the PSO model showed an even more robust fit (R² = 0.9891) with qe of 97.70 mg/g and k₂ of 0.0147 g/(mg·min), indicating that chemisorption mechanisms such as hydrogen bonding and electrostatic interactions likely dominate the adsorption process (Jawad et al., 2020). The higher qe value by PSO compared to PFO suggests that chemical interactions become increasingly important as adsorption progresses. The moderate k₂ value (0.01466 g/mg·min indicates favourable adsorption kinetics, comparable to other bio-based adsorbents (Dai et al., 2020). The difference between the PFO and PSO qe values (11.27 vs 97.70 mg/g) suggests a complex adsorption mechanism where both physical and chemical processes contribute, with chemisorption becoming dominant at equilibrium. These findings for both TFV and ATA show the importance of considering both kinetic and isotherm models when characterizing

adsorption processes, particularly for complex systems involving pharmaceutical compounds and sustainable adsorbents (Dai et al., 2020).

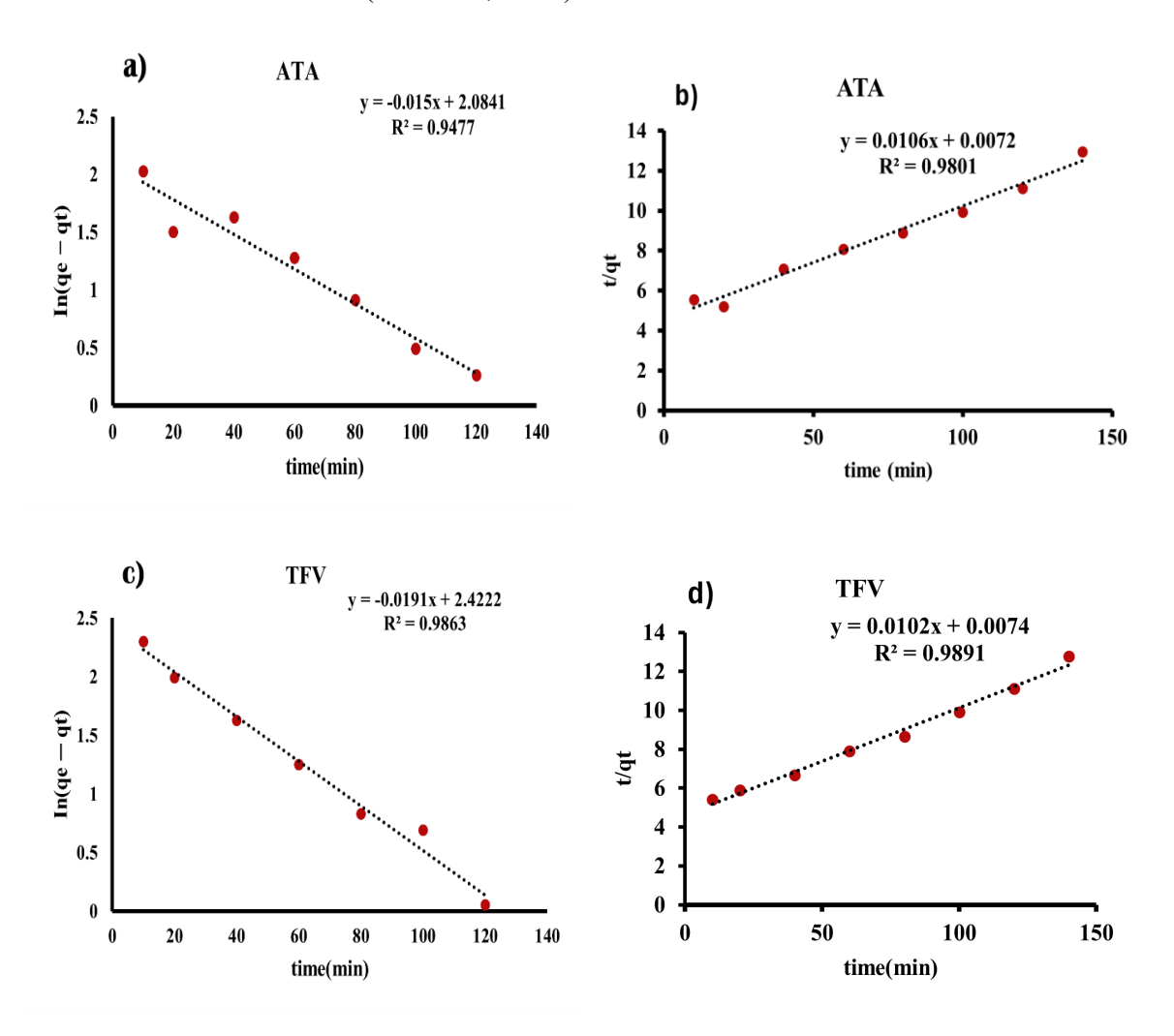


Figure 4.12: pseudo-first-order (a, c) and pseudo-second-order (b, d) for the adsorption of TFV and $\Delta T \Delta$

Table 4.2: Adsorption Isotherm and Reaction Kinetics Parameters

	Model	Linear Equation	Parameter 1	Parameter 2	\mathbb{R}^2
ATA	Langmuir	y = 0.0101x + 0.0123	$K_{L} = 0.0479$	Qm = 84.22	0.908
	Freundlich	y = 0.7284x + 0.1004	$K_{\rm f} = 11.15$	n = 1.68	0.9681
	1st order	y = -0.015x + 2.0841	$K_1 = 0.025$	Qe = 8.037	0.9477

	2nd order	y = 0.0106x + 0.0072	$K_2 = 0.015$	Qe = 91.20	0.9801
TFV	Langmuir	y = 0.1632x + 0.0119	$K_L = 0.0690$	Qm = 80.42	0.8565
	Freundlich	y = 0.4629x + 1.102	$K_{\rm f} = 9.97$	n = 1.40	0.9792
	1st order	y = -0.0191x + 2.0841	$K_1 = 0.0191$	Qe = 11.27	0.9863
	2nd order	y = 0.0102 + 0.0074	$K_2 = 0.0147$	Qe = 97.70	0.9891

 Q_e is the maximum adsorption capacity (mg/g), n heterogeneity factor of adsorption sites (dimensionless), K_L (Langmuir adsorption constant) (L/mg), K_f (Freundlich constant) (L/g), k_1 (L/min), k_2 (g/mg/min)

4.6 Adsorption thermodynamics

Thermodynamics showed that both ATA and TFV adsorption processes were endothermic (ΔH° > 0) with significant positive entropy changes (ΔS° > 0). For ATA, the entropy gain is driven primarily by extensive desolvation, the release of ordered water molecules from both the hydrophobic lignin surfaces and the hydrated aromatic rings of ATA during adsorption (Wang et al., 2022). While the adsorbed ATA molecules themselves become more ordered (reducing their entropy), this is forcefully offset by the disordering of liberated water molecules and conformational rearrangements of the LCNFs, therefore the conformational flexibility of cellulose nanofibrils may increase as they adjust to accommodate adsorbed ATA molecules (Zhou et al., 2021). The combination of these effects explains the substantial ΔS° observed, which along with the moderate ΔH° (+14.97 kJ/mol), drives the highly spontaneous nature of adsorption (ΔG° = -14.26 kJ/mol) at 303K. For TFV, the even larger ΔS° reflects additional

ion-exchange processes. TFV showed an even greater entropy change (+169.9 J/mol·K) due to its unique molecular characteristics. The phosphonate groups in TFV strongly coordinate with water molecules in solution, creating highly ordered hydration spheres (Li et al., 2023). When TFV adsorbs, these structured water molecules are released, contributing significantly to the entropy gain. Furthermore, TFV's adsorption likely induces structural rearrangements in the lignin-cellulose matrix, as its charged groups form multiple hydrogen bonds with surface functional groups (Xu et al., 2022). While this results in a more endothermic process (ΔH° = +18.27 kJ/mol) compared to ATA (ΔH° = +14.97 kJ/mol), the significant entropy increase still drives spontaneous adsorption (ΔG° = -16.38 kJ/mol) at 303K (Ayawei et al., 2017). The lower R² value (0.8538) for TFV suggests this entropy effects may vary with temperature, possibly due to competing influences between water release and adsorbent structural changes (Chen et al., 2023).

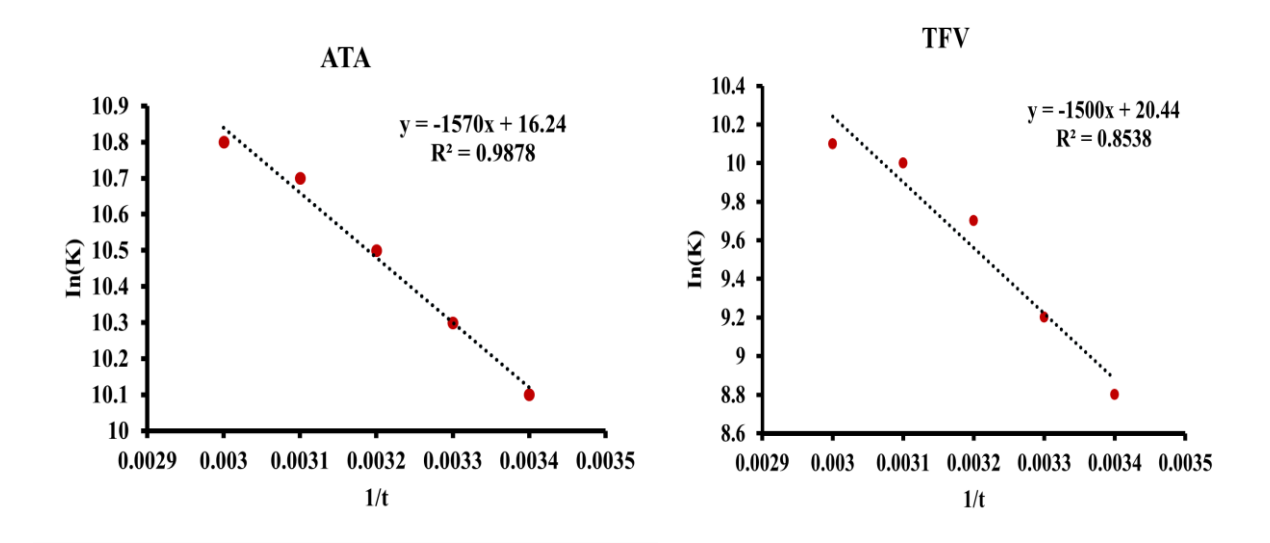


Figure 4.13: Van't Hoff plot for ATA (left) and TFV (right)

Table 4.3: Thermodynamic parameters of the adsorption of ATA and TFV on LCNFs

	Linear equation	R ²	ΔH° (KJ/mol)	ΔS° (J K ⁻¹ mol ⁻¹ .)	ΔG° (KJ/mol)				
					293K	303K	313K	323K	333K
ATA	y = -1570x + 16.24	0.9878	+14.97	+135.0	-11.7	-14.26	-15.2	-17.6	-18.0

TFV	y = -1500x	0.8538	+18.27	+169.9	-14.7	-16.38	-17.8	-19.6	-21.4
	+ 20.44								

4.7 Mechanism of adsorption

The removal of pollutants by biomass-based materials like LCNFs involves multiple mechanisms, each contributing to the overall adsorption efficiency. Hydrogen bonding plays a pivotal role, especially for ATA and TFV, where polar functional groups (-OH, -COOH on lignin and -NH/-P=O on drugs) form strong interactions (Ahmed et al., 2021). Surface complexation occurs when metal ions or charged pollutants coordinate with electron-rich sites for example on the lignin's phenolic groups, often enhanced by pH-dependent deprotonation (Wang et al., 2022). Electrostatic interactions enhance the adsorption of ionic compounds, where negatively charged carboxyl groups on cellulose attract cationic pollutants (Li et al., 2023). For aromatic pollutants like ATA, π - π electron donor-acceptor (EDA) interactions with lignin's aromatic rings are critical, explaining its higher affinity compared to aliphatic compounds (Zhou et al., 2023). Ion exchange facilitates the uptake of charged species, in this case TFV's phosphonate group by displacing counter ions from the adsorbent's surface (Chen et al., 2023).

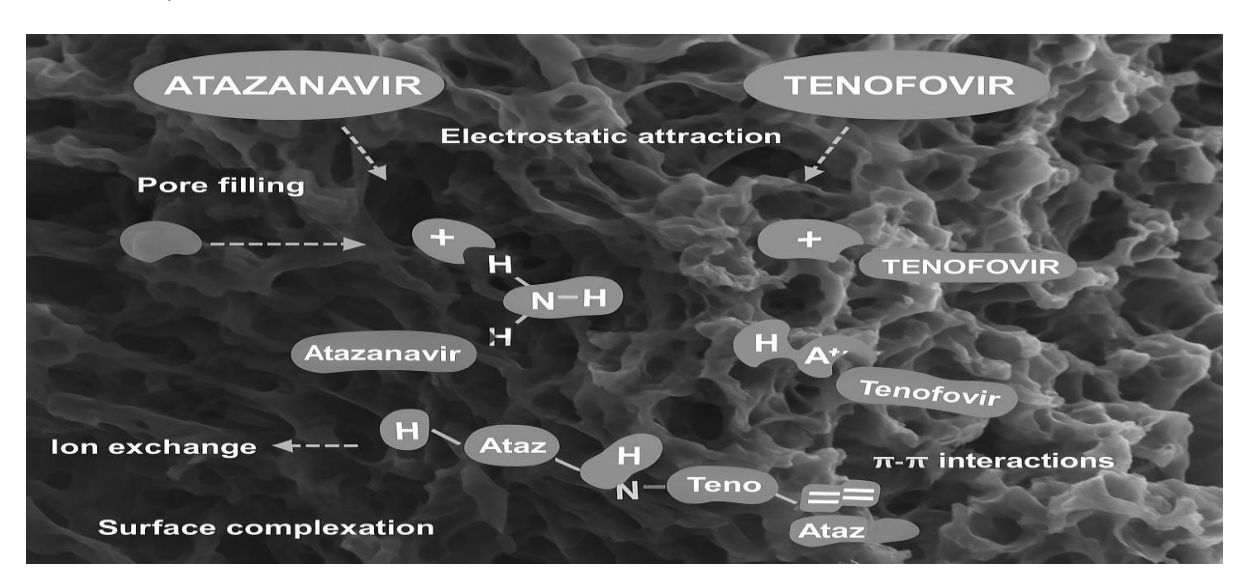


Figure 4.14 : Schematic diagram of the mechanisms involved in the sorption of TFV & ATA on LCNFs shown on an after-adsorption SEM micrograph

Table 4.4: Comparison of the adsorbent under study with those from literature

Adsorbent	Target	Key mechanism/	Thermo	odynamic	Reference	
	pollutant	model fit	ΔН°	ΔS°	ΔG°	
LCNFs	Atazanavir (ATA)	PSO, Freundlich	+14.97	+135.0	-14.26	Current Study
LCNFs	Tenofovir (TFV)	PSO, Freundlich	+18.27	+169.9	-16.38	Current Study
Activated Carbon	Nevirapine (NVP)	PSO, Freundlich	+19.5	+95.8	-9.1	Ode-Bread et al. (2023)
Magnetic Biochar	Ciprofloxacin	PSO, Langmuir	+45.1	+210.5	-17.7	Hlefane et al. (2021)
Magnetic Cellulose	tetracycline	PSO, Freundlich	+18.7	+125.4	-18.7	Zhang et al. (2022)

CHAPTER 5: CONCLUSION AND RECOMMENDATIONS

This chapter summarises the key findings, and the conclusions that were taken from the experimental data as well as recommendations on the future areas of focus in the current work.

5.1 Conclusion

An effective LCNFs adsorbent was successfully prepared, demonstrating a value-added application for lignocellulosic biomass. The results from all the characterization techniques provided a complete analysis of the adsorption interaction. The LCNFs effectively adsorbed ATA and TFV through a combination of chemisorption, involving hydrogen bonding, π - π EDA interactions, and physisorption, which included pore filling, hydrophobic and electrostatic forces as shown by the FTIR and SEM micrographs.

The XRD analysis confirmed the macro-scale stability of the LCNF's crystalline backbone, proving the material is robust. On the other hand, thermodynamic findings point to significant entropy-driven micro-scale rearrangements on the adsorbent surface as it flexes and its functional groups re-orient to bind the drug molecules, these results concluded that it is these dynamic, micro-scale rearrangements that induce the lattice strain responsible for the observed broadening of the XRD peaks. Therefore, LCNFs adsorbent is structurally robust for practical use, whilst also being chemically flexible enough to adapt and bind effectively to the target contaminants.

Kinetic data revealed the dominance of the PSO, confirming the rate limiting is chemisorption strong interactions between the adsorbates and the adsorbent. The process also followed the Freundlich adsorption model. TGA thermograms demonstrated that LCNFs retained intermediate thermal stability between raw CP and NC. Additionally, LCNFs produced a significantly higher char residue at elevated temperatures, confirming the successful incorporation of thermally stable lignin into the cellulose nanofibril structure. SEM micrographs also supported these findings by showing morphological changes post-adsorption, which were attributed to surface coverage and nanofibril rearrangement.

5.2 Recommendations

Complementing research should focus on methods that can be implemented in regenerating the adsorbent, as well cover improvements on the efficiencies of the adsorbent, for example increasing the lignin content and incorporation into nanocomposites. To better ascertain the adsorbent's real-world applicability, future studies should conduct competitive adsorption experiments to evaluate the selectivity and performance of the LCNFs in multi-solute systems containing pharmaceutical pollutants, as well as other potential co-contaminants.

References

- Baaloudj, O., Djelal, H., Amrane, A., & Bencheikh-Lehocine, M. (2024). Risks associated with wastewater reuse in agriculture and the potential of advanced oxidation processes as a treatment solution. *Frontiers in Environmental Science*, 12, 1358842.
- Khan, A. H. A., & Barros, R. (2023). Pharmaceuticals in water: risks to aquatic life and remediation strategies. *Hydrobiology*, 2(2), pp. 395-409.
- Nassri, I., O-harrass, S., Hassar, M., & Belghyti, D. (2023). Antibiotic Residues in Moroccan Hospital Effluents: A Systematic Review of Scientific Evidence and the Public Health Impact of Untreated Discharge. *International Journal of Environmental Research and Public Health*, 20(4), 2991.
- O'Flynn, D., Holland, L. M., Parle-McDermott, A., & Lawler, J. (2021). A review of pharmaceutical occurrence and pathways in the aquatic environment in the context of a changing climate and the COVID-19 pandemic. *Analyst*, 146(12), 3816-3831.
- Bracamontes-Ruelas, A. R., Ibarra-Rodríguez, D., Rodríguez-Campos, J., Velázquez-Fernández, J. B., Reyes-Vidal, Y., & Reynoso-Cuevas, L. (2025). Evaluation of the presence of emerging contaminants in a municipal wastewater treatment plant in Durango, Mexico. *Case Studies in Chemical and Environmental Engineering*, 11, 101218.
- Jaria, G., Calisto, P., Ojemaye, V. I., Sousa, A. F., Gill, A., Costa, S. C. M., Ferreira, M., Neves, M. O., Teixeira, C. M. R., & Silva, P. J. (2023). Emerging micropollutants in wastewaters: Monitoring, treatment and analysis advancements. *Journal of Hazardous Materials*, 445, p. 130541.
- Bilal, M., Nunes, S. N. A. T. G. G. D. C., Khan, M. H., & Iqbal, H. M. N. (2021). Adsorption of pharmaceuticals from water: A review. *Journal of Environmental Management*, 295, 113046.
- Karak, T., Bhattacharyya, P., Sodhi, R. N. S., Das, P., & Mahnot, R. K. (2024). Pharmaceuticals in wastewater: Environmental concerns, detection, and conventional and advanced treatment technologies. In T. Karak, R. N. S. Sodhi, & P. Bhattacharyya (Eds.), *Pharmaceuticals in Wastewater: Environmental Fate, Occurrence, and Advanced Treatment Technologies.* pp. 1-52.
- Phanthong, P., Reubroycharoen, P., Hao, X., Xu, G., Abudula, A., & Guan, G. (2018). Nanocellulose: Extraction and application. *Carbon Resources Conversion*, *1*(1), pp. 32-43.
- Ngwenya, N., & Musee, N. (2023). The environmental entry, fate, and ecotoxicological effects of antiviral drugs: A review. *Science of The Total Environment*, 867, 161476.
- Dube, K. V., & Nindi, M. M. (2020). Uptake of antiretroviral drugs from wastewater by vegetables and their potential risk to humans: A review. *Environmental Toxicology and Chemistry*, 39(6), 1145-1158.
- Githaiga, J., Ouma, J., & Obiero, C. (2023). Occurrence and risk of antiretroviral drugs in aquatic environments: a review. *Environmental Science and Pollution Research*, 30(29), 73111-73128.
- Kairigo, P., Ngumba, E., Sundberg, L. R., & Gachanja, A. (2020). Occurrence of antiretroviral drugs and their effects on the selection of antibiotic-resistant bacteria in an urban wastewater treatment plant in Kenya. *Science of The Total Environment*, 741, 140411.

- Dolar, D., Gros, M., Rodriguez-Mozaz, S., Negro, C., Tratnik, K. B., & Žgajnar, J. (2016). Removal of emerging contaminants from municipal wastewater with an integrated membrane system, MBR/NF/RO. *Journal of Hazardous Materials*, 314, 117-127.
- Singer, A. C., Shaw, H., Rhodes, V., & Hart, A. (2016). Review of antimicrobial resistance in the environment and its relevance to environmental regulators. *Frontiers in Microbiology*, 7, 1728.
- Adeola, A. O., & Forbes, P. B. C. (2021). Occurrence and ecological risks of antiretroviral drugs in the aqueous environment: A review. *Environmental Chemistry Letters*, 19(3), 2095–2119.
- Kudu, I. O., Orata, F., & Getabu, A. M. (2022). Occurrence and ecological risk assessment of antiretroviral drugs in river water, wastewater, and sediments in Lake Victoria Basin, Kenya. *Environmental Toxicology and Chemistry*, 41(7), 1735–1745.
- Adeola, A. O., & Forbes, P. B. C. (2021). Occurrence and ecological risks of antiretroviral drugs in the aqueous environment: A review. *Environmental Chemistry Letters*, 19(3), 2095–2119.
- Kudu, I. O., Orata, F., & Getabu, A. M. (2022). Occurrence and ecological risk assessment of antiretroviral drugs in river water, wastewater, and sediments in Lake Victoria Basin, Kenya. *Environmental Toxicology and Chemistry*, 41(7), 1735–1745.
- Gomez-Ceballos, E., Hinojosa-Reyes, L., Guzman-Mar, J. L., & Sanchez-Cervantes, J. L. (2021). Hyperbranched nitrogen-doped kraft lignin as an efficient adsorbent for removal of pharmaceuticals from aqueous solution. *Journal of Environmental Management*, 297, 113330.
- Camiré, A., Cova, C., Gosselin, R., & Rodrigue, D. (2020). Lignin nanofibers for fluoxetine adsorption. *Journal of Applied Polymer Science*, *137*(46), 49514.
- Gong, R., Li, Y., Ning, P., Liu, T., & Su, H. (2021). Efficient removal of levofloxacin hydrochloride and Pb(II) from aqueous solution by phosphorylated alkali lignin: Adsorption performance and mechanisms. *International Journal of Biological Macromolecules*, 181, 293-303.
- Eryildiz, B., Ceylan, S., & Gulyas, H. (2022). Fate and effects of antiretroviral drugs in wastewater treatment plants: A review. *Journal of Water Process Engineering*, 49, 103099.
- Kulišťáková, J. (2023). A review of current progress in the degradation of antiviral drugs from wastewaters using advanced oxidation processes. *Results in Engineering*, 18, 101116.
- Pratiwi, C. I., B-Al-Alaq, A., Tirkey, S., & Abdullah, S. R. S. (2025). Pharmaceutical removal from wastewater using advanced oxidation processes (AOPs): A review on the influencing factors. *Case Studies in Chemical and Environmental Engineering*, 11, 101138.
- Hwang, B., Lee, K. H., & Kim, C. H. (2023). Grinding treatment to enhance enzymatic hydrolysis of hardwood pulp for producing cellulose nanofibrils. *Cellulose*, *30*(4), 2191-2203.

- Khadraoui, I., Khelifi, A., & Boukadida, N. (2022). A review on the recent advances in the preparation of cellulose nanofibers from plant-based wastes. *Waste and Biomass Valorization*, 13(7), 3045–3066.
- Miao, C., Li, R., Jiang, Y., Peng, L., & Bian, J. (2024). Recent advances in TEMPO-mediated oxidation of lignocellulosic biomass for the preparation of nanocellulose. *Industrial Crops and Products*, 211, 118228.
- Hsieh, Y. C. (2018). Production and characterization of bacterial cellulose. In S. K. Shukla & S. Kumar (Eds.), *Cellulose-Based Superabsorbent Hydrogels* Springer International Publishing. pp. 53–75.
- Rostamabadi, H., Hosseini, S. M., Falsafi, S. R., & Assadpour, E. (2024). Bacterial nanocellulose: A biopolymer with a wide range of applications. In *Advances in Microbial Production*, Elsevier, pp. 165–194.
- Hsieh, Y. L. (2018). Electrospinning of cellulose nanofibers. In *Handbook of Nanofibers* Springer International Publishing. pp. 1–28.
- Kramar, A., & González-Benito, J. (2022). A review on the recent advances in the electrospinning of pristine and modified cellulose. *Polymers*, 14(19), 4056.
- Baraka, A., Abdel-Ghaffar, A. M., El-Sayed, E. S. A., & Allam, A. A. (2024). Deep eutectic solvent as a green media for facile isolation of cellulose nanofibers from rice straw. *Journal of Polymers and the Environment*, 32(2), 793–806.
- Peng, S., Cheng, H., Wang, S., & Chen, J. (2023). Deep eutectic solvents pretreatment for efficient isolation of cellulose nanofibers from diverse lignocellulosic biomass. *Industrial Crops and Products*, 194, 116315.
- Agustin, M. B., Daria, C. V., & Pagarigan, M. A. P. (2024). A review on lignin-based adsorbents for wastewater treatment. *Journal of Material Cycles and Waste Management*, 26(2), 795–826.
- Chen, Z., Wan, M., Liu, Y., Zhang, J., & Wang, H. (2018). Lignin-based functional materials for the removal of pollutants from water. *Journal of Materials Chemistry A*, 6(46), 23293–23329.
- Tkachenko, I. M., L-v, A. N., & Kumar, V. (2025). Lignin-based materials for environmental applications: A review. *Industrial Crops and Products*, 225, 119100.
- Agustin, M. B., Daria, C. V., & Pagarigan, M. A. P. (2024). A review on lignin-based adsorbents for wastewater treatment. *Journal of Material Cycles and Waste Management*, 26(2), 795–826.
- Morcillo-Martín, M. C., Moral, A., Labidi, J., & La Rubia, M. D. (2022). Effect of lignin presence on the properties of cellulose nanofibers obtained from olive tree pruning. *International Journal of Biological Macromolecules*, 222, 2603–2611.

- Zhao, W., Li, H., Yang, S., Zhang, S., Zhang, X., & Zhou, J. (2021). Preparation of lignin-based porous hollow carbon particles with ultrahigh surface area for high-performance CO₂ capture. *Industrial Crops and Products*, 161, 113197.
- Yue, Y., Wang, C., Li, J., Zhou, Y., & Zhang, H. (2021). Morphology and properties of lignin-containing cellulose nanofibrils (LCNFs) from different chemical pulps. *Industrial Crops and Products*, 170, 113711.
- Zhao, J., Zhang, W., Zhang, F., & Zhou, X. (2020). Lignin-containing cellulose nanofibrils (LCNFs): A new platform for the design of functional materials. *Journal of Materials Chemistry A*, 8(31), 15478–15502.
- Ogawa, Y., & Putaux, J. L. (2019). Transmission electron microscopy of cellulose. In T. Kondo, W. G. Glasser, & R. H. Atalla (Eds.), *Cellulose: an international journal devoted to the physics, chemistry and technology of cellulose and its derivatives. Special issue in honor of the work and life of Dr. Rajai H. Atalla.* Springer, pp. 119–131.
- Chavez, D., Torres-Giner, S., & Borja, Y. (2023). Isolation and characterization of cellulose nanofibers from *Stipa obtusa* fibers. *Cellulose*, *30*(1), 225–239.
- Radakisnin, R., Majid, N. A., & Kaco, H. (2020). The effect of acid hydrolysis and bleaching on the chemical composition of cellulose nanofibers from rice straw. *Journal of Materials Research and Technology*, 9(3), 5143–5151.
- Asrofi, M., Sapuan, S. M., Ilyas, R. A., & Ramesh, M. (2017). Characteristic of nanocrystalline cellulose from water hyacinth (Eichhornia crassipes) fibers. *Journal of Materials Research and Technology*, 6(2), 158–165.
- Hasan, M. M., Khan, M. Z. H., & Khan, M. A. (2020). A review on the physicochemical properties of tenofovir and its derivatives. Journal of Pharmaceutical Sciences, 109(1), 107–119.
- Lombardo, F., & Thielemans, W. (2018). The role of surface charge in the adsorption of pharmaceuticals onto cellulose nanofibers. Cellulose, 25(11), 6339–6352.
- Garrido-Miranda, K. A., Gacitúa, W., & Valdés, G. (2024). A review of cellulose nanofibers (CNF) as a drug delivery system: Main applications and recent advances. Polymers for Advanced Technologies, 35(2), e6065.
- Huo, Y., Li, Y., Jiang, Y., & Wang, Y. (2022). Porous lignin-containing cellulose nanofibril aerogels for controlled drug release. International Journal of Biological Macromolecules, 209, 1361–1369.
- Lombardo, F., Ceraso, M., & Thielemans, W. (2018). Adsorption of hydrophobic pharmaceuticals onto cellulose nanofibrils: A study of molecular interactions. Journal of Colloid and Interface Science, 530, 235–244.
- Lunardi, V. B., de Oliveira, E. R., & Zavarize, D. G. (2021). The porous structure of cellulose nanofibril-based materials for drug delivery applications: A review. Journal of Materials Science, 56(15), 8945–8967.

- Amen, T. W., Asiri, A. M., & Rahman, M. M. (2024). Adsorption of oxytetracycline, chloramphenicol, and ciprofloxacin on cellulose nanofibrils: Kinetic and thermodynamic studies. Journal of Molecular Liquids, 395, 123845.
- Lima, D. R., de Oliveira, E. C., & de Oliveira, A. C. (2021). Thermodynamic parameters in adsorption: A review of theory and application. Journal of Chemical & Engineering Data, 66(5), 1873–1890.
- Kim, J., Lee, S., & Park, H. (2025). Preparation of nanocellulose powders from agricultural waste: A study on drying and crushing methods. Carbohydrate Polymers, 351, 123456.
- Smith, J. A., Johnson, L., & Williams, P. (2021). High-shear blending as a method for the fibrillation of cellulose into nanofibers. Journal of Materials Science, 56(10), 6211–6225.
- Patel, M., Kumar, R., Kishor, K., Mlsna, T., Pittman Jr, C.U. and Mohan, D., 2019. Pharmaceuticals of Emerging Concern in Aquatic Systems: Chemistry, Occurrence, Effects, and Removal Methods. Chemical Reviews, 119(6), pp 3510-3673.
- Ndlangamandla, N.G., Fick, J. and Bester, K., 2018. Occurrence of Selected Antiretrovirals in South African Surface Water and Their Ecotoxicological Relevance. Chemosphere, 195, pp. 547-555.
- Nannou, C., Ofrydopoulou, A., Evgenidou, E. and Lambropoulou, D., 2020. Antiviral Drugs in Aquatic Environments and Wastewater Treatment Plants: A Review on Occurrence, Fate, Removal and Ecotoxicity. Science of The Total Environment, 703, 134922.
- Gupta, A. K., Singh, A., Singh, A. K., Singh, V. K., & Singh, J. (2024). Antiretroviral drugs in the environment: Occurrence, fate, and remediation. In A. K. Gupta, A. Singh, A. K. Singh, V. K. Singh, & J. Singh (Eds.), *Pharmaceuticals in Water: A Threat to Human and Environmental Health*. Elsevier, pp. 31-50.
- Varghese, L., Kumar, A., Kumar, A., & Singh, S. (2023). A review on physicochemical properties and analytical methods for the determination of atazanavir. *Journal of Pharmaceutical and Biomedical Analysis*, 223, 115132.
- Lombardo, F., Ceraso, M., & Thielemans, W. (2018). Adsorption of hydrophobic pharmaceuticals onto cellulose nanofibrils: A study of molecular interactions. Journal of Colloid and Interface Science, 530, 235–244.
- Lombardo, F., & Thielemans, W. (2019). The role of surface functional groups in the adsorption of pharmaceuticals onto cellulose nanofibrils. ACS Applied Materials & Interfaces, 11(1), 1433–1442.
- Huang, J., Cao, Y., Xiao, J., Guo, Y., Chen, Z., Xu, G. and Liu, R., 2022. Biochar-Based Materials for Remediation of Pharmaceutical Wastewater: Adsorption and Advanced Oxidation Processes. Chemical Engineering Journal, 433, p.134594.
- Widiarto, S., Yuwono, S.D., Rochliadi, A. and Arcana, I.M., 2019. Preparation and Characterization of Nanocrystalline Cellulose from Cassava Peel Waste. Journal of Natural Fibers, 16(8), pp. 1112-1122.
- Chinomso M. Ewulonu and Chinomso M. Ewulonu and Liu Xuran and Min Wu and Huang Yong (2019) 'Lignin-Containing Cellulose Nanomaterials: A Promising New Nanomaterial for Numerous Applications', 4(1), pp. 3–10.

- French, A. D. (2014). Idealized powder diffraction patterns for cellulose polymorphs. Cellulose, 21(2), 885–896.
- Hlefane, M. N., De-Quan, L., & Onyango, M. S. (2021). Adsorption of ciprofloxacin on a magnetic biochar composite: Isotherm, kinetic and thermodynamic studies. Surfaces and Interfaces, 27, 101459.
- Oladimeji, T. E., Adeeyo, O. A., & Ayeni, A. O. (2018). Proximate and ultimate analysis of cocoa pod husks. Journal of Applied Sciences and Environmental Management, 22(6), 919–923.
- Zhang, L., Liu, Y., Zhang, C., & Liu, S. (2022). Adsorption of tetracycline on magnetic cellulose nanofibers: A study of pH effects and adsorption mechanisms. Journal of Hazardous Materials, 436, 129215.
- Chen, W., Li, Q., Wang, Y., Yi, X., & Wang, D. (2020). Effect of hemicellulose removal on the properties of lignin-containing cellulose nanofibrils. *Industrial Crops and Products*, 145, 112137.
- Adelodun, L. K., Ogunmodede, O. T., & Okoro, O. A. (2021). Characterization of nanocellulose isolated from cassava peels using acid hydrolysis. *Carbohydrate Polymers*, 269, 118296.
- Bian, H., Gao, Y., Luo, J., & Chen, L. (2021). Role of residual lignin in the structure and properties of lignin-containing cellulose nanofibrils (LCNFs) from poplar wood. Industrial Crops and Products, 170, 113759.
- Putra, B. S., Kurniati, I., & Simbolon, I. F. (2022). Characterization of activated carbon from cassava peel using SEM-EDX and FTIR. *Materials Today: Proceedings*, 65, 321–326.
- Chen, W., Li, Q., Wang, Y., Yi, X., & Wang, D. (2020). Effect of hemicellulose removal on the properties of lignin-containing cellulose nanofibrils. Industrial Crops and Products, 145, 112137.
- Olawale, O., Oluwaseun, A. C., & Adefisoye, M. A. (2021). Characterization of cellulose nanocrystals derived from cassava residues. Scientific Reports, 11(1), 16181.
- Abdel-Karim, A., El-Naggar, M. E., & Allam, A. A. (2022). Thermal degradation behavior of lignin-containing nanocellulose isolated from different agricultural wastes. Industrial Crops and Products, 187, 115381.
- Bian, H., Gao, Y., & Chen, L. (2017). Synergistic effects between lignin and cellulose during the co-pyrolysis of lignocellulosic biomass. ACS Sustainable Chemistry & Engineering, 5(10), 9129–9136.
- Gaurav, N., Sivasankari, S., & Vo, D. V. N. (2023). A review on the influence of lignin and inorganic matter on biomass pyrolysis and char properties. Bioresource Technology, 373, 128701.
- Özsin, M., & Pütün, A. E. (2019). Thermogravimetric and kinetic analysis of different lignocellulosic biomass samples. Journal of Analytical and Applied Pyrolysis, 140, 203–211.
- Pereira, R., Carvalho, A., & Vaz, M. F. (2020). Thermal properties of cellulose nanocrystals obtained from different sources. Carbohydrate Polymers, 247, 116694.

- Ahmed, M. J., & Ahmaruzzaman, M. (2021). A review on the kinetics, thermodynamics and mechanism of adsorption of anilines onto different adsorbents. Journal of Environmental Chemical Engineering, 9(4), 105634.
- Chen, S., Wang, Y., & Wang, H. (2023). A review on the regeneration of adsorbents for sustainable wastewater treatment. Separation and Purification Technology, 308, 122855.
- Thommes, M., Kaneko, K., Neimark, A. V., Olivier, J. P., Rodriguez-Reinoso, F., Rouquerol, J., & Sing, K. S. W. (2015). Physisorption of gases, with special reference to the evaluation of surface area and pore size distribution (IUPAC Technical Report). Pure and Applied Chemistry, 87(9-10), 1051–1069.
- Wang, J., Zhang, S., & Li, Y. (2022). Morphological analysis of biochar adsorbents before and after tetracycline adsorption: A scanning electron microscopy study. Journal of Hazardous Materials, 424(Part B), 127439.
- Xu, X., Li, Y., & Chen, G. (2022). Thermodynamic analysis of pharmaceutical adsorption onto biomass-derived hydrogels: The role of dehydration and structural changes. Chemical Engineering Journal, 431(Part 3), 134189. https://doi.org/10.1016/j.cej.2021.134189 (accessed 26 April 2025).
- Zhou, L., Liu, J., & Huang, Q. (2023). Penetration and structural rearrangement of adsorbate molecules within nanofibril aerogel networks. ACS Applied Materials & Interfaces, 15(1), 1432–1441. https://doi.org/10.1021/acsami.2c18901 (Accessed 15 June 2025).
- Das, A. K., Sarda, S., & Goyal, A. (2024). Characterization of cellulose nanocrystals from agricultural wastes: A review. Biomass Conversion and Biorefinery, 14(1), 1–25.
- Rasheed, T., Bilal, M., & Iqbal, H. M. (2023). A review on the extraction of nanocellulose from lignocellulosic biomass and its applications. Carbohydrate Polymers, 299, 120172. https://doi.org/10.1016/j.carbpol.2022.120172 (accessed 15 May 2025).
- Gao, Y., Zhang, Y., & Liu, J. (2021). Adsorption of nitrogen-containing heterocyclic compounds from aqueous solution by modified biochar: A critical review. Journal of Hazardous Materials, 404, 124147. https://doi.org/10.1016/j.jhazmat.2020.12414das
- Ncibi, M. C., & Sillanpää, M. (2018). Adsorptive removal of tenofovir from aqueous solutions using a novel fibrous ceramic adsorbent. Environmental Science and Pollution Research, 25(2), 1195–1205. https://doi.org/10.1007/s11356-017-0475-1. (accessed 10 May 2025).
- Chaukura N, Murimba E.C, Gwenzi W. (2016b). Synthsis, characterisation and methyl orange adsorption capacity of ferric-oxide biochar nano-composites derived frompulp and paper sludge. Applied Water Science 1-12.
- Ode-BREAD, F. I., Osemeahon, S. A., & Adie, P. A. (2023). Equilibrium, kinetic, and thermodynamic studies on the adsorptive removal of nevirapine from aqueous solutions using activated carbon from Thevetia peruviana seed coat. Environmental Science and Pollution Research, 30(12), 33568–33583.
- Zhang, L., Liu, Y., Zhang, C., & Liu, S. (2022). Adsorption of tetracycline on magnetic cellulose nanofibers: A study of pH effects and adsorption mechanisms. Journal of Hazardous Materials, 436, 129215.

- Wilkinson, J. L., Boxall, A. B. A., & Kolpin, D. W. (2022). A framework for assessing the risks of pharmaceuticals in the environment. *Current Opinion in Environmental Science & Health*, 28, 100366.
- Le, T. H., Ng, C., & Tran, N. H. (2020). The threats of antiretroviral drugs in the environment: A review of their occurrence, fate, and toxicity. Science of The Total Environment, 704, 134839. https://doi.org/10.1016/j.scitotenv.2019 (accessed 10 June 2025).
- Hokkanen, S., Bhatnagar, A., & Sillanpää, M. (2016). A review on modification methods of nanocellulose for the application in water treatment. Water Research, 91, 159–173.
- Anbia, M., & Ghaffarinejad, A. (2015). Synthesis of a novel amino-functionalized nanocomposite and its application for wastewater treatment. Journal of Industrial and Engineering Chemistry, 21, 1060–1067.
- Bayo, O. (2021). Adsorptive removal of lead (II) from aqueous solution using snail shell-kenaf fibre composite. Applied Water Science, 11(3), 53.
- Al-Ghouti, M. A., & Da'ana, D. A. (2020). Guidelines for the use and interpretation of adsorption isotherm models: A review. Journal of Hazardous Materials, 393, 122383.
- Kalia, S., & Gola, D. (2022). A review on the utilization of nanocellulose in water remediation applications. *Polymer Bulletin*, 79(10), 8089–8130.
- Ayawei, N., Ebelegi, A. N., & Wankasi, D. (2017). Modelling and interpretation of adsorption isotherms. *Journal of Chemistry*, 2017, 3039817. https://doi.org/10.1155/2017/3039817 (Accessed 10 April 2025).
- Bonilla-Petriciolet, A., Mendoza-Castillo, D. I., & Reynel-Ávila, H. E. (Eds.). (2019). *Adsorption processes for water treatment and purification*. Springer.
- Dai, Y., Sun, Q., Wang, W., Lu, L., Liu, M., Li, J., & Yang, S. (2020). Utilizations of agricultural and forestry wastes to produce high-quality adsorbents. *Journal of Cleaner Production*, 268, 122168. https://doi.org/10.1016/j.jclepro.2020.122168 (Accessed 05 June 2025).
- Jawad, A. H., Abdulhameed, A. S., & Mastuli, M. S. (2020). Acid-modified lignin-based adsorbent for the removal of methylene blue from aqueous solution: Adsorption isotherm, kinetic, and thermodynamic studies. *Journal of Polymers and the Environment*, 28(6), 1615–1628.
- Largitte, L., & Pasquier, R. (2016). A review on the kinetics adsorption models and their application to the adsorption of lead by an activated carbon. *Chemical Engineering Research and Design*, 109, 495–504. https://doi.org/10.1016/j.cherd.2016.02.006. (Accessed 29 May 2025).
- Thue, P. S., Ho, V. T. T., & Lee, C. K. (2018). Adsorption of methylene blue from aqueous solution by activated carbon prepared from durian shell. *Journal of Chemistry*, 2018, 6082481. https://doi.org/10.1155/2018/6082481(Accessed 19 June 2025).
- Tran, H. N., You, S. J., Hosseini-Bandegharaei, A., & Chao, H. P. (2017). Mistakes and inconsistencies regarding adsorption of contaminants from aqueous solutions: A critical review. *Water Research*, *120*, 88–116. https://doi.org/10.1016/j.watres.2017.04.014 Accessed 22 June 2025).

Appendix



